Supernova Neutrino Burst Detection with the Deep Underground Neutrino Experiment

B. Abi[140], R. Acciarri[61], M. A. Acero[8], G. Adamov[65], D. Adams[17], M. Adinolfi[16], Z. Ahmad[179], J. Ahmed[182], T. Alion[168], S. Alonso Monsalve[21], C. Alt[53], J. Anderson[4], C. Andreopoulos[157,117], M. P. Andrews[61], F. Andrianala[2], S. Andringa[113], A. Ankowski[158], M. Antonova[77], S. Antusch[10], A. Aranda-Fernandez[39], A. Ariga[11], L. O. Arnold[42], M. A. Arroyave[52], J. Asaadi[172], A. Aurisano[37], V. Aushev[112], D. Autiero[89], F. Azfar[140], H. Back[141], J. J. Back[182], C. Backhouse[177], P. Baesso[16], L. Bagby[61], R. Bajou[143], S. Balasubramanian[186], P. Baldi[26], B. Bambah[75], F. Barao[113,91], G. Barenboim[77], G. J. Barker[182], W. Barkhouse[134], C. Barnes[124], G. Barr[140], J. Barranco Monarca[70], N. Barros[113,55], J. L. Barrow[170,61], A. Bashyal[139], V. Basque[122], F. Bay[133], J. L. Bazo Alba[150], J. F. Beacom[138], E. Bechetoille[89], B. Behera[41], L. Bellantoni[61], G. Bellettini[148], V. Bellini[33,79], O. Beltramello[21], D. Belver[22], N. Benekos[21], F. Bento Neves[113], J. Berger[149], S. Berkman[61], P. Bernardini[81,160], R. M. Berner[11], H. Berns[25], S. Bertolucci[78,14], M. Betancourt[61], Y. Bezawada[25], M. Bhattacharjee[95], B. Bhuyan[95], S. Biagi[87], J. Bian[26], M. Biassoni[82], K. Biery[61], B. Bilki[12,99], M. Bishai[17], A. Bitadze[122], A. Blake[115], B. Blanco Siffert[60], F. D. M. Blaszczyk[61], G. C. Blazey[135], E. Blucher[35], J. Boissevain[118], S. Bolognesi[20], T. Bolton[109], M. Bonesini[82,126], M. Bongrand[114], F. Bonini[17], A. Booth[168], C. Booth[162], S. Bordoni[21], A. Borkum[168], T. Boschi[51], N. Bostan[99], P. Bour[44], S. B. Boyd[182], D. Boyden[135], J. Bracinik[13], D. Braga[61], D. Brailsford[115], A. Brandt[172], J. Bremer[21], C. Brew[157], E. Brianne[122], S. J. Brice[61], C. Brizzolari[82,126], C. Bromberg[125], G. Brooijmans[42], J. Brooke[16], A. Bross[61], G. Brunetti[85], N. Buchanan[41], H. Budd[154], D. Caiulo[89], P. Calafiura[116], J. Calcutt[125], M. Calin[18], S. Calvez[41], E. Calvo[22], L. Camilleri[42], A. Caminata[80], M. Campanelli[177], D. Caratelli[61], G. Carini[17], B. Carlus[89], P. Carniti[82], I. Caro Terrazas[41], H. Carranza[172], A. Castillo[161], C. Castromonte[98], C. Cattadori[82], F. Cavalier[114], F. Cavanna[61], S. Centro[142], G. Cerati[61], A. Cervelli[78], A. Cervera Villanueva[77], M. Chalifour[21], C. Chang[28], E. Chardonnet[143], A. Chatterjee[149], S. Chattopadhyay[179], J. Chaves[145], H. Chen[17], M. Chen[26], Y. Chen[11], D. Cherdack[74], C. Chi[42], S. Childress[61], A. Chiriacescu[18], K. Cho[107], S. Choubey[71], A. Christensen[41], D. Christian[61], G. Christodoulou[21], E. Church[141], P. Clarke[54], T. E. Coan[166], A. G. Cocco[84], J. A. B. Coelho[114], E. Conley[50], J. M. Conrad[123], M. Convery[158], L. Corwin[163], P. Cotte[20], L. Cremaldi[130], L. Cremonesi[177], J. I. Crespo-Anadón[22], E. Cristaldo[6], R. Cross[115], C. Cuesta[22], Y. Cui[28], D. Cussans[16], M. Dabrowski[17], H. da Motta[19], L. Da Silva Peres[60], C. David[61,188], Q. David[89], G. S. Davies[130], S. Davini[80], J. Dawson[143], K. De[172], R. M. De Almeida[63], P. Debbins[99], I. De Bonis[47], M. P. Decowski[133,1], A. de Gouvêa[136], P. C. De Holanda[32], I. L. De Icaza Astiz[168], A. Deisting[155], P. De Jong[133,1], A. Delbart[20], D. Delepine[70], M. Delgado[3], A. Dell'Acqua[21], P. De Lurgio[4], J. R. T. de Mello Neto[60], D. M. DeMuth[178], S. Dennis[31], C. Densham[157], G. Deptuch[61], A. De Roeck[21], V. De Romeri[77], J. J. De Vries[31], R. Dharmapalan[73], M. Dias[176], F. Diaz[150], J. S. Díaz[97], S. Di Domizio[80,64], L. Di Giulio[21], P. Ding[61], L. Di Noto[80,64], C. Distefano[87], R. Diurba[129], M. Diwan[17], Z. Djurcic[4], N. Dokania[167], M. J. Dolinski[49], L. Domine[158], D. Douglas[125], F. Drielsma[158], D. Duchesneau[47], K. Duffy[61], P. Dunne[94], T. Durkin[157], H. Duyang[165], O. Dvornikov[73], D. A. Dwyer[116], A. S. Dyshkant[135], M. Eads[135], D. Edmunds[125], J. Eisch[100], S. Emery[20], A. Ereditato[11], C. O. Escobar[61], L. Escudero Sanchez[31], J. J. Evans[122], E. Ewart[97], A. C. Ezeribe[162], K. Fahey[61], A. Falcone[82,126], C. Farnese[142], Y. Farzan[90], J. Felix[70], E. Fernandez-Martinez[121], P. Fernandez Menendez[77], F. Ferraro[80,64], L. Fields[61], A. Filkins[184], F. Filthaut[133,153], R. S. Fitzpatrick[124], W. Flanagan[46], B. Fleming[186], R. Flight[154], J. Fowler[50], W. Fox[97], J. Franc[44], K. Francis[135], D. Franco[186], J. Freeman[61], J. Freestone[122], J. Fried[17], A. Friedland[158], S. Fuess[61], I. Furic[62], A. P. Furmanski[129], A. Gago[150], H. Gallagher[175], A. Gallego-Ros[22], N. Gallice[83,127], V. Galymov[89], E. Gamberini[21], T. Gamble[162], R. Gandhi[71], R. Gandrajula[125], S. Gao[17], D. Garcia-Gamez[68], M. Á. García-Peris[77], S. Gardiner[61], D. Gastler[15], G. Ge[42], B. Gelli[32], A. Gendotti[53], S. Gent[164], Z. Ghorbani-Moghaddam[80],

D. Gibin[142], I. Gil-Botella[22], C. Girerd[89], A. K. Giri[96], D. Gnani[116], O. Gogota[112], M. Gold[131], S. Gollapinni[118], K. Gollwitzer[61], R. A. Gomes[57], L. V. Gomez Bermeo[161], L. S. Gomez Fajardo[161], F. Gonnella[13], J. A. Gonzalez-Cuevas[6], M. C. Goodman[4], O. Goodwin[122], S. Goswami[147], C. Gotti[82], E. Goudzovski[13], C. Grace[116], M. Graham[158], E. Gramellini[186], R. Gran[128], E. Granados[70], A. Grant[48], C. Grant[15], D. Gratieri[63], P. Green[122], S. Green[31], L. Greenler[185], M. Greenwood[139], J. Greer[16], W. C. Griffith[168], M. Groh[97], J. Grudzinski[4], K. Grzelak[181], W. Gu[17], V. Guarino[4], R. Guenette[72], A. Guglielmi[85], B. Guo[165], K. K. Guthikonda[108], R. Gutierrez[3], P. Guzowski[122], M. M. Guzzo[32], S. Gwon[36], A. Habig[128], A. Hackenburg[186], H. Hadavand[172], R. Haenni[11], A. Hahn[61], J. Haigh[182], J. Haiston[163], T. Hamernik[61], P. Hamilton[94], J. Han[149], K. Harder[157], D. A. Harris[61,188], J. Hartnell[168], T. Hasegawa[106], R. Hatcher[61], E. Hazen[15], A. Heavey[61], K. M. Heeger[186], J. Heise[159], K. Hennessy[117], S. Henry[154], M. A. Hernandez Morquecho[70], K. Herner[61], L. Hertel[26], A. S. Hesam[21], J. Hewes[37], A. Higuera[74], T. Hill[92], S. J. Hillier[13], A. Himmel[61], J. Hoff[61], C. Hohl[10], A. Holin[177], E. Hoppe[141], G. A. Horton-Smith[109], M. Hostert[51], A. Hourlier[123], B. Howard[61], R. Howell[154], J. Huang[173], J. Huang[25], J. Hugon[119], G. Iles[94], N. Ilic[174], A. M. Iliescu[78], R. Illingworth[61], A. Ioannisian[187], R. Itay[158], A. Izmaylov[77], E. James[61], B. Jargowsky[26], F. Jediny[44], C. Jesùs-Valls[76], X. Ji[17], L. Jiang[180], S. Jiménez[22], A. Jipa[18], A. Joglekar[28], C. Johnson[41], R. Johnson[37], B. Jones[172], S. Jones[177], C. K. Jung[167], T. Junk[61], Y. Jwa[42], M. Kabirnezhad[140], A. Kaboth[157], I. Kadenko[112], F. Kamiya[59], G. Karagiorgi[42], A. Karcher[116], M. Karolak[20], Y. Karyotakis[47], S. Kasai[111], S. P. Kasetti[119], L. Kashur[41], N. Kazaryan[187], E. Kearns[15], P. Keener[145], K.J. Kelly[61], E. Kemp[32], W. Ketchum[61], S. H. Kettell[17], M. Khabibullin[88], A. Khotjantsev[88], A. Khvedelidze[65], D. Kim[21], B. King[61], B. Kirby[17], M. Kirby[61], J. Klein[145], K. Koehler[185], L. W. Koerner[74], S. Kohn[24,116], P. P. Koller[11], M. Kordosky[184], T. Kosc[89], U. Kose[21], V. A. Kostelecký[97], K. Kothekar[16], F. Krennrich[100], I. Kreslo[11], Y. Kudenko[88], V. A. Kudryavtsev[162], S. Kulagin[88], J. Kumar[73], R. Kumar[152], C. Kuruppu[165], V. Kus[44], T. Kutter[119], A. Lambert[116], K. Lande[145], C. E. Lane[49], K. Lang[173], T. Langford[186], P. Lasorak[168], D. Last[145], C. Lastoria[22], A. Laundrie[185], A. Lawrence[116], I. Lazanu[18], R. LaZur[41], T. Le[175], J. Learned[73], P. LeBrun[89], G. Lehmann Miotto[21], R. Lehnert[97], M. A. Leigui de Oliveira[59], M. Leitner[116], M. Leyton[76], L. Li[26], S. Li[17], S. W. Li[158], T. Li[54], Y. Li[17], H. Liao[109], C. S. Lin[116], S. Lin[119], A. Lister[185], B. R. Littlejohn[93], J. Liu[26], S. Lockwitz[61], T. Loew[116], M. Lokajicek[43], I. Lomidze[65], K. Long[94], K. Loo[105], D. Lorca[11], T. Lord[182], J. M. LoSecco[137], W. C. Louis[118], K.B. Luk[24,116], X. Luo[29], N. Lurkin[13], T. Lux[76], V. P. Luzio[59], D. MacFarland[158], A. A. Machado[32], P. Machado[61], C. T. Macias[97], J. R. Macier[61], A. Maddalena[67], P. Madigan[24,116], S. Magill[4], K. Mahn[125], A. Maio[113,55], A. Major[50], J. A. Maloney[45], G. Mandrioli[78], J. Maneira[113,55], L. Manenti[177], S. Manly[154], A. Mann[175], K. Manolopoulos[157], M. Manrique Plata[97], A. Marchionni[61], W. Marciano[17], D. Marfatia[73], C. Mariani[180], J. Maricic[73], F. Marinho[58], A. D. Marino[40], M. Marshak[129], C. Marshall[116], J. Marshall[182], J. Marteau[89], J. Martin-Albo[77], N. Martinez[109], D.A. Martinez Caicedo [163], S. Martynenko[167], K. Mason[175], A. Mastbaum[156], M. Masud[77], S. Matsuno[73], J. Matthews[119], C. Mauger[145], N. Mauri[78,14], K. Mavrokoridis[117], R. Mazza[82], A. Mazzacane[61], E. Mazzucato[20], E. McCluskey[61], N. McConkey[122], K. S. McFarland[154], C. McGrew[167], A. McNab[122], A. Mefodiev[88], P. Mehta[103], P. Melas[7], M. Mellinato[82,126], O. Mena[77], S. Menary[188], H. Mendez[151], A. Menegolli[86,144], G. Meng[85], M. D. Messier[97], W. Metcalf[119], M. Mewes[97], H. Meyer[183], T. Miao[61], G. Michna[164], T. Miedema[133,153], J. Migenda[162], R. Milincic[73], W. Miller[129], J. Mills[175], C. Milne[92], O. Mineev[88], O. G. Miranda[38], S. Miryala[17], C. S. Mishra[61], S. R. Mishra[165], A. Mislivec[129], D. Mladenov[21], I. Mocioiu[146], K. Moffat[51], N. Moggi[78,14], R. Mohanta[75], T. A. Mohayai[61], N. Mokhov[61], J. Molina[6], L. Molina Bueno[53], A. Montanari[78], C. Montanari[86,144], D. Montanari[61], L. M. Montano Zetina[38], J. Moon[123], M. Mooney[41], A. Moor[31], D. Moreno[3], B. Morgan[182], C. Morris[74], C. Mossey[61], E. Motuk[177], C. A. Moura[59], J. Mousseau[124], W. Mu[61], L. Mualem[30], J. Mueller[41], M. Muether[183], S. Mufson[97], F. Muheim[54], A. Muir[48], M. Mulhearn[25], H. Muramatsu[129], S. Murphy[53], J. Musser[97], J. Nachtman[99], S. Nagu[120], M. Nalbandyan[187], R. Nandakumar[157], D. Naples[149], S. Narita[101], D. Navas-Nicolás[22], N. Nayak[26], M. Nebot-Guinot[54], L. Necib[30], K. Negishi[101], J. K. Nelson[184], J. Nesbit[185], M. Nessi[21], D. Newbold[157], M. Newcomer[145], D. Newhart[61], R. Nichol[177], E. Niner[61], K. Nishimura[73], A. Norman[61], A. Norrick[61], R. Northrop[35], P. Novella[77], J. A. Nowak[115], M. Oberling[4], A. Olivares

Del Campo[51], A. Olivier[154], Y. Onel[99], Y. Onishchuk[112], J. Ott[26], L. Pagani[25], S. Pakvasa[73],
O. Palamara[61], S. Palestini[21], J. M. Paley[61], M. Pallavicini[80,64], C. Palomares[22], E. Pantic[25],
V. Paolone[149], V. Papadimitriou[61], R. Papaleo[87], A. Papanestis[157], S. Paramesvaran[16], S. Parke[61],
Z. Parsa[17], M. Parvu[18], S. Pascoli[51], L. Pasqualini[78,14], J. Pasternak[94], J. Pater[122], C. Patrick[177],
L. Patrizii[78], R. B. Patterson[30], S. J. Patton[116], T. Patzak[143], A. Paudel[109], B. Paulos[185],
L. Paulucci[59], Z. Pavlovic[61], G. Pawloski[129], D. Payne[117], V. Pec[162], S. J. M. Peeters[168],
Y. Penichot[20], E. Pennacchio[89], A. Penzo[99], O. L. G. Peres[32], J. Perry[54], D. Pershey[50], G. Pessina[82],
G. Petrillo[158], C. Petta[33,79], R. Petti[165], F. Piastra[11], L. Pickering[125], F. Pietropaolo[85,21],
J. Pillow[182], J. Pinzino[174], R. Plunkett[61], R. Poling[129], X. Pons[21], N. Poonthottathil[100], S. Pordes[61],
M. Potekhin[17], R. Potenza[33,79], B. V. K. S. Potukuchi[102], J. Pozimski[94], M. Pozzato[78,14],
S. Prakash[32], T. Prakash[116], S. Prince[72], G. Prior[113], D. Pugnere[89], K. Qi[167], X. Qian[17],
J. L. Raaf[61], R. Raboanary[2], V. Radeka[17], J. Rademacker[16], B. Radics[53], A. Rafique[4], E. Raguzin[17],
M. Rai[182], M. Rajaoalisoa[37], I. Rakhno[61], H. T. Rakotondramanana[2], L. Rakotondravohitra[2],
Y. A. Ramachers[182], R. Rameika[61], M. A. Ramirez Delgado[70], B. Ramson[61], A. Rappoldi[86,144],
G. Raselli[86,144], P. Ratoff[115], S. Ravat[21], H. Razafinime[2], J.S. Real[69], B. Rebel[185,61], D. Redondo[22],
M. Reggiani-Guzzo[32], T. Rehak[49], J. Reichenbacher[163], S. D. Reitzner[61], A. Renshaw[74],
S. Rescia[17], F. Resnati[21], A. Reynolds[140], G. Riccobene[87], L. C. J. Rice[149], K. Rielage[118],
Y. Rigaut[53], D. Rivera[145], L. Rochester[158], M. Roda[117], P. Rodrigues[140], M. J. Rodriguez Alonso[21],
J. Rodriguez Rondon[163], A. J. Roeth[50], H. Rogers[41], S. Rosauro-Alcaraz[121], M. Rossella[86,144],
J. Rout[103], S. Roy[71], A. Rubbia[53], C. Rubbia[66], B. Russell[116], J. Russell[158], D. Ruterbories[154],
R. Saakyan[177], S. Sacerdoti[143], T. Safford[125], N. Sahu[96], P. Sala[83,21], N. Samios[17], M. C. Sanchez[100],
D. A. Sanders[130], D. Sankey[157], S. Santana[151], M. Santos-Maldonado[151], N. Saoulidou[7],
P. Sapienza[87], C. Sarasty[37], I. Sarcevic[5], G. Savage[61], V. Savinov[149], A. Scaramelli[86], A. Scarff[162],
A. Scarpelli[17], T. Schaffer[128], H. Schellman[139,61], P. Schlabach[61], D. Schmitz[35], K. Scholberg[50],
A. Schukraft[61], E. Segreto[32], J. Sensenig[145], I. Seong[26], A. Sergi[13], F. Sergiampietri[167],
D. Sgalaberna[53], M. H. Shaevitz[42], S. Shafaq[103], M. Shamma[28], H. R. Sharma[102], R. Sharma[17],
T. Shaw[61], C. Shepherd-Themistocleous[157], S. Shin[104], D. Shooltz[125], R. Shrock[167], L. Simard[114],
N. Simos[17], J. Sinclair[11], G. Sinev[50], J. Singh[120], J. Singh[120], V. Singh[23,9], R. Sipos[21],
F. W. Sippach[42], G. Sirri[78], A. Sitraka[163], K. Siyeon[36], D. Smargianaki[167], A. Smith[31], E. Smith[97],
P. Smith[97], J. Smolik[44], M. Smy[26], P. Snopok[93], M. Soares Nunes[32], H. Sobel[26], M. Soderberg[169],
C. J. Solano Salinas[98], S. Söldner-Rembold[122], N. Solomey[183], V. Solovov[113], W. E. Sondheim[118],
M. Sorel[77], J. Soto-Oton[22], A. Sousa[37], K. Soustruznik[34], F. Spagliardi[140], M. Spanu[17], J. Spitz[124],
N. J. C. Spooner[162], K. Spurgeon[169], R. Staley[13], M. Stancari[61], L. Stanco[85], H. M. Steiner[116],
J. Stewart[17], B. Stillwell[35], J. Stock[163], F. Stocker[21], T. Stokes[119], M. Strait[129], T. Strauss[61],
S. Striganov[61], A. Stuart[39], D. Summers[130], A. Surdo[81], V. Susic[10], L. Suter[61], C. M. Sutera[33,79],
R. Svoboda[25], B. Szczerbinska[171], A. M. Szelc[122], R. Talaga[4], H. A. Tanaka[158], B. Tapia Oregui[173],
A. Tapper[94], S. Tariq[61], E. Tatar[92], R. Tayloe[97], A. M. Teklu[167], M. Tenti[78], K. Terao[158],
C. A. Ternes[77], F. Terranova[82,126], G. Testera[80], A. Thea[157], J. L. Thompson[162], C. Thorn[17],
S. C. Timm[61], A. Tonazzo[143], M. Torti[82,126], M. Tortola[77], F. Tortorici[33,79], D. Totani[61],
M. Toups[61], C. Touramanis[117], J. Trevor[30], W. H. Trzaska[105], Y. T. Tsai[158], Z. Tsamalaidze[65],
K. V. Tsang[158], N. Tsverava[65], S. Tufanli[21], C. Tull[116], E. Tyley[162], M. Tzanov[119], M. A. Uchida[31],
J. Urheim[97], T. Usher[158], M. R. Vagins[110], P. Vahle[184], G. A. Valdiviesso[56], E. Valencia[184],
Z. Vallari[30], J. W. F. Valle[77], S. Vallecorsa[21], R. Van Berg[145], R. G. Van de Water[118], D. Vanegas
Forero[32], F. Varanini[85], D. Vargas[76], G. Varner[73], J. Vasel[97], G. Vasseur[20], K. Vaziri[61],
S. Ventura[85], A. Verdugo[22], S. Vergani[31], M. A. Vermeulen[133], M. Verzocchi[61], H. Vieira de
Souza[32], C. Vignoli[67], C. Vilela[167], B. Viren[17], T. Vrba[44], T. Wachala[132], A. V. Waldron[94],
M. Wallbank[37], H. Wang[27], J. Wang[25], Y. Wang[27], Y. Wang[167], K. Warburton[100], D. Warner[41],
M. Wascko[94], D. Waters[177], A. Watson[13], P. Weatherly[49], A. Weber[157,140], M. Weber[11], H. Wei[17],
A. Weinstein[100], D. Wenman[185], M. Wetstein[100], M. R. While[163], A. White[172], L. H. Whitehead[31],
D. Whittington[169], M. J. Wilking[167], C. Wilkinson[11], Z. Williams[172], F. Wilson[157], R. J. Wilson[41],
J. Wolcott[175], T. Wongjirad[175], K. Wood[167], L. Wood[141], E. Worcester[17], M. Worcester[17],
C. Wret[154], W. Wu[61], W. Wu[26], Y. Xiao[26], G. Yang[167], T. Yang[61], N. Yershov[88], K. Yonehara[61],
T. Young[134], B. Yu[17], J. Yu[172], R. Zaki[188], J. Zalesak[43], L. Zambelli[47], B. Zamorano[68], A. Zani[83],

L. Zazueta[184], G. P. Zeller[61], J. Zennamo[61], K. Zeug[185], C. Zhang[17], M. Zhao[17], E. Zhivun[17], G. Zhu[138], E. D. Zimmerman[40], M. Zito[20], S. Zucchelli[78,14], J. Zuklin[43], V. Zutshi[135], R. Zwaska[61]

[1]University of Amsterdam, NL-1098 XG Amsterdam, The Netherlands
[2] University of Antananarivo, Antananarivo 101, Madagascar
[3] Universidad Antonio Nariño, Bogotá, Colombia
[4] Argonne National Laboratory, Argonne, IL 60439, USA
[5] University of Arizona, Tucson, AZ 85721, USA
[6] Universidad Nacional de Asunción, San Lorenzo, Paraguay
[7] University of Athens, Zografou GR 157 84, Greece
[8] Universidad del Atlántico, Atlántico, Colombia
[9] Banaras Hindu University, Varanasi - 221 005, India
[10] University of Basel, CH-4056 Basel, Switzerland
[11] University of Bern, CH-3012 Bern, Switzerland
[12] Beykent University, Istanbul, Turkey
[13] University of Birmingham, Birmingham B15 2TT, United Kingdom
[14] Università del Bologna, 40127 Bologna, Italy
[15] Boston University, Boston, MA 02215, USA
[16] University of Bristol, Bristol BS8 1TL, United Kingdom
[17] Brookhaven National Laboratory, Upton, NY 11973, USA
[18] University of Bucharest, Bucharest, Romania
[19] Centro Brasileiro de Pesquisas Físicas, Rio de Janeiro, RJ 22290-180, Brazil
[20] CEA/Saclay, IRFU Institut de Recherche sur les Lois Fondamentales de l'Univers, F-91191 Gif-sur-Yvette CEDEX, France
[21] CERN, The European Organization for Nuclear Research, 1211 Meyrin, Switzerland
[22] CIEMAT, Centro de Investigaciones Energéticas, Medioambientales y Tecnológicas, E-28040 Madrid, Spain
[23] Central University of South Bihar, Gaya – 824236, India
[24] University of California Berkeley, Berkeley, CA 94720, USA
[25] University of California Davis, Davis, CA 95616, USA
[26] University of California Irvine, Irvine, CA 92697, USA
[27] University of California Los Angeles, Los Angeles, CA 90095, USA
[28] University of California Riverside, Riverside CA 92521, USA
[29] University of California Santa Barbara, Santa Barbara, California 93106 USA
[30] California Institute of Technology, Pasadena, CA 91125, USA
[31] University of Cambridge, Cambridge CB3 0HE, United Kingdom
[32] Universidade Estadual de Campinas, Campinas - SP, 13083-970, Brazil
[33] Università di Catania, 2 - 95131 Catania, Italy
[34] Institute of Particle and Nuclear Physics of the Faculty of Mathematics and Physics of the Charles University, 180 00 Prague 8, Czech Republic
[35] University of Chicago, Chicago, IL 60637, USA
[36] Chung-Ang University, Seoul 06974, South Korea
[37] University of Cincinnati, Cincinnati, OH 45221, USA
[38] Centro de Investigación y de Estudios Avanzados del Instituto Politécnico Nacional (Cinvestav), Mexico City, Mexico
[39] Universidad de Colima, Colima, Mexico
[40] University of Colorado Boulder, Boulder, CO 80309, USA
[41] Colorado State University, Fort Collins, CO 80523, USA
[42] Columbia University, New York, NY 10027, USA
[43] Institute of Physics, Czech Academy of Sciences, 182 00 Prague 8, Czech Republic
[44] Czech Technical University, 115 19 Prague 1, Czech Republic
[45] Dakota State University, Madison, SD 57042, USA
[46] University of Dallas, Irving, TX 75062-4736, USA
[47] Laboratoire d'Annecy-le-Vieux de Physique des Particules, CNRS/IN2P3 and Université Savoie Mont Blanc, 74941 Annecy-le-Vieux, France
[48] Daresbury Laboratory, Cheshire WA4 4AD, United Kingdom
[49] Drexel University, Philadelphia, PA 19104, USA
[50] Duke University, Durham, NC 27708, USA
[51] Durham University, Durham DH1 3LE, United Kingdom
[52] Universidad EIA, Antioquia, Colombia
[53] ETH Zurich, Zurich, Switzerland
[54] University of Edinburgh, Edinburgh EH8 9YL, United Kingdom
[55] Faculdade de Ciências da Universidade de Lisboa - FCUL, 1749-016 Lisboa, Portugal
[56] Universidade Federal de Alfenas, Poços de Caldas - MG, 37715-400, Brazil
[57] Universidade Federal de Goias, Goiania, GO 74690-900, Brazil
[58] Universidade Federal de São Carlos, Araras - SP, 13604-900, Brazil
[59] Universidade Federal do ABC, Santo André - SP, 09210-580 Brazil
[60] Universidade Federal do Rio de Janeiro, Rio de Janeiro - RJ, 21941-901, Brazil
[61] Fermi National Accelerator Laboratory, Batavia, IL 60510, USA
[62] University of Florida, Gainesville, FL 32611-8440, USA
[63] Fluminense Federal University, 9 Icaraí Niterói - RJ, 24220-900, Brazil
[64] Università degli Studi di Genova, Genova, Italy
[65] Georgian Technical University, Tbilisi, Georgia
[66] Gran Sasso Science Institute, L'Aquila, Italy

[67] Laboratori Nazionali del Gran Sasso, L'Aquila AQ, Italy
[68] University of Granada & CAFPE, 18002 Granada, Spain
[69] University Grenoble Alpes, CNRS, Grenoble INP, LPSC-IN2P3, 38000 Grenoble, France
[70] Universidad de Guanajuato, Guanajuato, C.P. 37000, Mexico
[71] Harish-Chandra Research Institute, Jhunsi, Allahabad 211 019, India
[72] Harvard University, Cambridge, MA 02138, USA
[73] University of Hawaii, Honolulu, HI 96822, USA
[74] University of Houston, Houston, TX 77204, USA
[75] University of Hyderabad, Gachibowli, Hyderabad - 500 046, India
[76] Institut de Fìsica d'Altes Energies, Barcelona, Spain
[77] Instituto de Fisica Corpuscular, 46980 Paterna, Valencia, Spain
[78] Istituto Nazionale di Fisica Nucleare Sezione di Bologna, 40127 Bologna BO, Italy
[79] Istituto Nazionale di Fisica Nucleare Sezione di Catania, I-95123 Catania, Italy
[80] Istituto Nazionale di Fisica Nucleare Sezione di Genova, 16146 Genova GE, Italy
[81] Istituto Nazionale di Fisica Nucleare Sezione di Lecce, 73100 - Lecce, Italy
[82] Istituto Nazionale di Fisica Nucleare Sezione di Milano Bicocca, 3 - I-20126 Milano, Italy
[83] Istituto Nazionale di Fisica Nucleare Sezione di Milano, 20133 Milano, Italy
[84] Istituto Nazionale di Fisica Nucleare Sezione di Napoli, I-80126 Napoli, Italy
[85] Istituto Nazionale di Fisica Nucleare Sezione di Padova, 35131 Padova, Italy
[86] Istituto Nazionale di Fisica Nucleare Sezione di Pavia, I-27100 Pavia, Italy
[87] Istituto Nazionale di Fisica Nucleare Laboratori Nazionali del Sud, 95123 Catania, Italy
[88] Institute for Nuclear Research of the Russian Academy of Sciences, Moscow 117312, Russia
[89] Institut de Physique des 2 Infinis de Lyon, 69622 Villeurbanne, France
[90] Institute for Research in Fundamental Sciences, Tehran, Iran
[91] Instituto Superior Técnico - IST, Universidade de Lisboa, Portugal
[92] Idaho State University, Pocatello, ID 83209, USA
[93] Illinois Institute of Technology, Chicago, IL 60616, USA
[94] Imperial College of Science Technology and Medicine, London SW7 2BZ, United Kingdom
[95] Indian Institute of Technology Guwahati, Guwahati, 781 039, India
[96] Indian Institute of Technology Hyderabad, Hyderabad, 502285, India
[97] Indiana University, Bloomington, IN 47405, USA
[98] Universidad Nacional de Ingeniería, Lima 25, Perú
[99] University of Iowa, Iowa City, IA 52242, USA
[100] Iowa State University, Ames, Iowa 50011, USA
[101] Iwate University, Morioka, Iwate 020-8551, Japan
[102] University of Jammu, Jammu-180006, India
[103] Jawaharlal Nehru University, New Delhi 110067, India
[104] Jeonbuk National University, Jeonrabuk-do 54896, South Korea
[105] University of Jyvaskyla, FI-40014, Finland
[106] High Energy Accelerator Research Organization (KEK), Ibaraki, 305-0801, Japan
[107] Korea Institute of Science and Technology Information, Daejeon, 34141, South Korea
[108] K L University, Vaddeswaram, Andhra Pradesh 522502, India
[109] Kansas State University, Manhattan, KS 66506, USA
[110] Kavli Institute for the Physics and Mathematics of the Universe, Kashiwa, Chiba 277-8583, Japan
[111] National Institute of Technology, Kure College, Hiroshima, 737-8506, Japan
[112] Kyiv National University, 01601 Kyiv, Ukraine
[113] Laboratório de Instrumentação e Física Experimental de Partículas, 1649-003 Lisboa and 3004-516 Coimbra, Portugal
[114] Laboratoire de l'Accélérateur Linéaire, 91440 Orsay, France
[115] Lancaster University, Lancaster LA1 4YB, United Kingdom
[116] Lawrence Berkeley National Laboratory, Berkeley, CA 94720, USA
[117] University of Liverpool, L69 7ZE, Liverpool, United Kingdom
[118] Los Alamos National Laboratory, Los Alamos, NM 87545, USA
[119] Louisiana State University, Baton Rouge, LA 70803, USA
[120] University of Lucknow, Uttar Pradesh 226007, India
[121] Madrid Autonoma University and IFT UAM/CSIC, 28049 Madrid, Spain
[122] University of Manchester, Manchester M13 9PL, United Kingdom
[123] Massachusetts Institute of Technology, Cambridge, MA 02139, USA
[124] University of Michigan, Ann Arbor, MI 48109, USA
[125] Michigan State University, East Lansing, MI 48824, USA
[126] Università del Milano-Bicocca, 20126 Milano, Italy
[127] Università degli Studi di Milano, I-20133 Milano, Italy
[128] University of Minnesota Duluth, Duluth, MN 55812, USA
[129] University of Minnesota Twin Cities, Minneapolis, MN 55455, USA
[130] University of Mississippi, University, MS 38677 USA
[131] University of New Mexico, Albuquerque, NM 87131, USA
[132] H. Niewodniczański Institute of Nuclear Physics, Polish Academy of Sciences, Cracow, Poland
[133] Nikhef National Institute of Subatomic Physics, 1098 XG Amsterdam, Netherlands
[134] University of North Dakota, Grand Forks, ND 58202-8357, USA
[135] Northern Illinois University, DeKalb, Illinois 60115, USA
[136] Northwestern University, Evanston, Il 60208, USA
[137] University of Notre Dame, Notre Dame, IN 46556, USA

[138] Ohio State University, Columbus, OH 43210, USA
[139] Oregon State University, Corvallis, OR 97331, USA
[140] University of Oxford, Oxford, OX1 3RH, United Kingdom
[141] Pacific Northwest National Laboratory, Richland, WA 99352, USA
[142] Universtà degli Studi di Padova, I-35131 Padova, Italy
[143] Université de Paris, CNRS, Astroparticule et Cosmologie, F-75006, Paris, France
[144] Università degli Studi di Pavia, 27100 Pavia PV, Italy
[145] University of Pennsylvania, Philadelphia, PA 19104, USA
[146] Pennsylvania State University, University Park, PA 16802, USA
[147] Physical Research Laboratory, Ahmedabad 380 009, India
[148] Università di Pisa, I-56127 Pisa, Italy
[149] University of Pittsburgh, Pittsburgh, PA 15260, USA
[150] Pontificia Universidad Católica del Perú, Lima, Perú
[151] University of Puerto Rico, Mayaguez 00681, Puerto Rico, USA
[152] Punjab Agricultural University, Ludhiana 141004, India
[153] Radboud University, NL-6525 AJ Nijmegen, Netherlands
[154] University of Rochester, Rochester, NY 14627, USA
[155] Royal Holloway College London, TW20 0EX, United Kingdom
[156] Rutgers University, Piscataway, NJ, 08854, USA
[157] STFC Rutherford Appleton Laboratory, Didcot OX11 0QX, United Kingdom
[158] SLAC National Accelerator Laboratory, Menlo Park, CA 94025, USA
[159] Sanford Underground Research Facility, Lead, SD, 57754, USA
[160] Università del Salento, 73100 Lecce, Italy
[161] Universidad Sergio Arboleda, 11022 Bogotá, Colombia
[162] University of Sheffield, Sheffield S3 7RH, United Kingdom
[163] South Dakota School of Mines and Technology, Rapid City, SD 57701, USA
[164] South Dakota State University, Brookings, SD 57007, USA
[165] University of South Carolina, Columbia, SC 29208, USA
[166] Southern Methodist University, Dallas, TX 75275, USA
[167] Stony Brook University, SUNY, Stony Brook, New York 11794, USA
[168] University of Sussex, Brighton, BN1 9RH, United Kingdom
[169] Syracuse University, Syracuse, NY 13244, USA
[170] University of Tennessee at Knoxville, TN, 37996, USA
[171] Texas A&M University - Corpus Christi, Corpus Christi, TX 78412, USA
[172] University of Texas at Arlington, Arlington, TX 76019, USA
[173] University of Texas at Austin, Austin, TX 78712, USA
[174] University of Toronto, Toronto, Ontario M5S 1A1, Canada
[175] Tufts University, Medford, MA 02155, USA
[176] Universidade Federal de São Paulo, 09913-030, São Paulo, Brazil
[177] University College London, London, WC1E 6BT, United Kingdom
[178] Valley City State University, Valley City, ND 58072, USA
[179] Variable Energy Cyclotron Centre, 700 064 West Bengal, India
[180] Virginia Tech, Blacksburg, VA 24060, USA
[181] University of Warsaw, 00-927 Warsaw, Poland
[182] University of Warwick, Coventry CV4 7AL, United Kingdom
[183] Wichita State University, Wichita, KS 67260, USA
[184] William and Mary, Williamsburg, VA 23187, USA
[185] University of Wisconsin Madison, Madison, WI 53706, USA
[186] Yale University, New Haven, CT 06520, USA
[187] Yerevan Institute for Theoretical Physics and Modeling, Yerevan 0036, Armenia
[188] York University, Toronto M3J 1P3, Canada

August 18, 2020

Abstract The Deep Underground Neutrino Experiment (DUNE), a 40-kton underground liquid argon time projection chamber experiment, will be sensitive to the electron-neutrino flavor component of the burst of neutrinos expected from the next Galactic core-collapse supernova. Such an observation will bring unique insight into the astrophysics of core collapse as well as into the properties of neutrinos. The general capabilities of DUNE for neutrino detection in the relevant few- to few-tens-of-MeV neutrino energy range will be described. As an example, DUNE's ability to constrain the ν_e spectral parameters of the neutrino burst will be considered.

1 Introduction

The Deep Underground Neutrino Experiment (DUNE) will be made up of four 10-kton liquid argon time projection chambers underground in South Dakota as part of the DUNE/Long-Baseline Neutrino Facility (LNBF) program. DUNE will record and reconstruct neutrino interactions in the $\sim$GeV and higher range for studies of neutrino oscillation parameters and searches for new physics using neutrinos from a beam sent from Fermilab and using neutrinos from the atmosphere. DUNE's dynamic range is such that it is also sensitive to neutrinos with energies down to about 5 MeV. Charged-current (CC) interactions of neutrinos from around 5 MeV to several tens of MeV create short electron tracks in liquid argon, potentially accompanied by gamma-ray and other secondary particle signatures. This regime is of particular interest for detection of the burst of neutrinos from a galactic core-collapse supernova. Such a detection would be of great interest in the context of multi-messenger astronomy. The sensitivity of DUNE is primarily to electron-flavor neutrinos from supernovae, and this capability is unique among existing and proposed supernova neutrino detectors for the next decades. Neutrinos and antineutrinos from other astrophysical sources, such as solar and diffuse supernova background neutrinos, are also potentially detectable. This low-energy (few to few tens of MeV) event regime has particular reconstruction, background and triggering challenges.

One of the primary physics goals of DUNE as stated in the Technical Design Report (TDR) [1,2,3] is to "Detect and measure the ν_e flux from a core-collapse supernova within our galaxy, should one occur during the lifetime of the DUNE experiment. Such a measurement would provide a wealth of unique information about the early stages of core collapse, and could even signal the birth of a black hole." [4].

This paper will describe selected studies from the DUNE TDR aimed at understanding DUNE's sensitivity to low-energy neutrino physics, with an emphasis on supernova burst signals. Section 2 describes basic supernova neutrino physics. Section 3 gives an overview of the landscape of supernova neutrino burst detection. Section 4 gives a brief description of the DUNE far detector. Section 5 describes the general properties of low-energy events in DUNE, including interaction channels, tools developed so far, and backgrounds. The tools include MARLEY, a neutrino event generator specifically developed for this energy regime [5], and the SNOw-GLoBES fast event-rate calculation tool [6]. These are both open-source community tools, rather than DUNE-specific software. Section 5.3 describes the expected supernova signal in DUNE, and Sec. 5.4 describes burst triggering. Section 6 describes astrophysics of the collapse, explosion and remnant to be learned from the burst. Section 7 gives an overview of neutrino physics that can be extracted from a supernova burst observation. Details on supernova pointing capabilities and solar neutrino capabilities will be described in separate publications.

2 Supernova neutrino bursts

2.1 Neutrinos from Collapsed Stellar Cores: Basics

A core-collapse supernova[1] occurs when a massive star reaches the end of its life. As a result of nuclear burning throughout the star's life, the central region of such a star gains an "onion" structure, with an iron core at the center surrounded by concentric shells of lighter elements (silicon, oxygen, neon, magnesium, carbon, etc). At temperatures of $T \sim 10^{10}$ K and densities of $\rho \sim 10^{10}$ g/cm^3, the Fe core continuously loses energy by neutrino emission (through pair annihilation and plasmon decay [7]). Since iron cannot be further burned, the lost energy cannot be replenished throughout the volume and the core continues to contract and heat up, while also growing in mass thanks to the shell burning. Eventually, the critical mass of about $1.4M_\odot$ of Fe is reached, at which point a stable configuration is no longer possible. As electrons are absorbed by the protons in nuclei and some iron is disintegrated by thermal photons, the degeneracy pressure support is suddenly removed and the core collapses essentially in free

---

[1] "Supernova" always refers to a "core-collapse supernova" in this paper, although we are aware that not all core collapses produce electromagnetically visible supernovae, and not all supernovae result from stellar core collapse.

fall, reaching speeds of about a quarter of the speed of light[2].

The collapse of the central region is suddenly halted after $\sim 10^{-2}$ seconds, as the density reaches nuclear (or super-nuclear) values. The central core rebounds and an outward-moving shock wave is formed. The extreme physical conditions of this core, in particular the densities of order $10^{12} - 10^{14}$ g/cm^3, create a medium that is opaque even for neutrinos. As a consequence, the core initially has a trapped lepton number. The gravitational energy of the collapse at this stage is stored mostly in the degenerate Fermi sea of electrons ($E_F \sim 200$ MeV) and electron neutrinos, which are in equilibrium with the former. The temperature of this core is not more than 30 MeV, which means the core is relatively cold.

At the next stage, the trapped energy and lepton number both escape from the core, carried by the least interacting particles, which in the standard model are neutrinos. Neutrinos and antineutrinos of all flavors are emitted in a time span of a few seconds (their diffusion time). The resulting central object then settles to a neutron star, or a black hole. A tremendous amount of energy, some 10^{53} ergs, is released in 10^{58} neutrinos with energies ~ 10 MeV. A fraction of this energy is absorbed by beta reactions into the material behind the shock wave that then blasts away the rest of the star, creating, in many cases, a spectacular explosion. Yet, from the energetics point of view, this visible explosion is but a tiny perturbation on the total event. Over 99% of all gravitational binding energy of the $1.4 M_\odot$ collapsed core – some 10% of its rest mass – is emitted in neutrinos.

2.2 Stages of the Explosion

The core-collapse neutrino signal starts with a short, sharp "neutronization" (or "break-out") burst primarily composed of ν_e from $e^- + p \rightarrow \nu_e + n$. These neutrinos are messengers of the shock front breaking through the neutrinosphere (the surface of neutrino trapping): when this happens, iron is disintegrated, the neutrino scattering rate drops and the lepton number trapped just below the original neutrinosphere is suddenly released. This quick and intense burst is followed by an "accretion" phase lasting some hundreds of milliseconds, depending on the progenitor star mass, as matter falls onto the collapsed core and the shock is stalled at the distance of ~ 200 km. The gravitational binding energy

[2]Other collapse mechanisms are possible: an "electron-capture" supernova does not reach the final burning phase before highly degenerate electrons break apart nuclei and trigger a collapse.

of the accreting material is powering the neutrino luminosity during this stage. The later "cooling" phase over ~ 10 seconds represents the main part of the signal, over which the proto-neutron star sheds its trapped energy.

The flavor content and spectra of the neutrinos emitted from the neutrinosphere change throughout these phases, and the supernova's evolution can be followed with the neutrino signal.
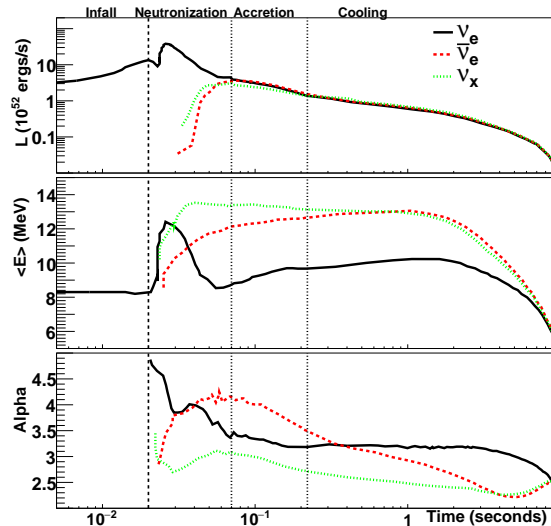

Fig. 1 Expected time-dependent flux parameters for a specific model for an electron-capture supernova [8]. No flavor transitions are assumed. The top plot shows the luminosity as a function of time, the second plot shows average neutrino energy, and the third plot shows the α (pinching) parameter. The vertical dashed line at 0.02 seconds indicates the time of core bounce, and the vertical lines indicate different eras in the supernova evolution. The leftmost time interval indicates the infall period. The next interval, from core bounce to 50 ms, is the neutronization burst era, in which the flux is composed primarily of ν_e. The next period, from 50 to 200 ms, is the accretion period. The final era, from 0.2 to 9 seconds, is the proto-neutron-star cooling period. The general features are qualitatively similar for most core-collapse supernova models.

The physics of neutrino decoupling and spectra formation is far from trivial, owing to the energy dependence of the cross sections and the roles played by both CC and neutral-current (NC) reactions. Detailed transport calculations using methods such as MC or Boltzmann solvers have been employed. It has been observed that flux spectra coming out of such simulations can typically be parameterized at a given moment in time by the following ansatz (e.g., [10,11]):

$$\phi(E_\nu) = \mathcal{N} \left(\frac{E_\nu}{\langle E_\nu \rangle} \right)^\alpha \exp \left[-(\alpha + 1) \frac{E_\nu}{\langle E_\nu \rangle} \right] , \qquad (1)$$

where E_ν is the neutrino energy, $\langle E_\nu \rangle$ is the mean neutrino energy, α is a "pinching parameter", and $\mathcal{N}$ is
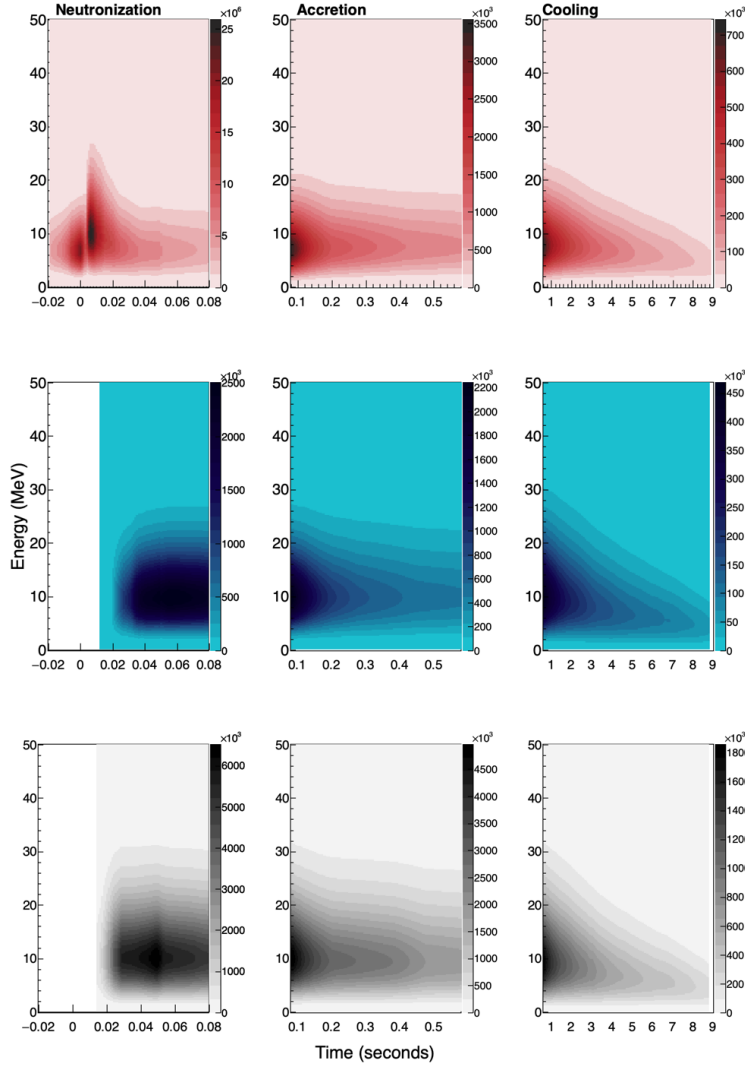
Fig. 2 Examples of time-dependent neutrino spectra for the electron-capture supernova model [8] parameterized in Fig. 1, on three different timescales. The x-axis for all plots indicates time in seconds and the y-axis indicates neutrino energy in MeV. The z-axis color-shading units are neutrinos per cm^2 per millisecond per 0.2 MeV. Note the different z scales in the panels. Core bounce is at $t = 0$. Top: ν_e. Center: $\bar{\nu}_e$. Bottom: ν_x. Flavor transition effects are not included here; note they can have dramatic effects on the spectra. Figure modified from Ref. [9].

a normalization constant related to the total luminosity. Large α corresponds to a more "pinched" spectrum (suppressed tails at high and low energy). This parameterization is referred to as a "pinched-thermal" form. The different ν_e, $\bar{\nu}_e$ and ν_x ($x = \mu, \tau, \bar{\mu}, \bar{\tau}$) flavors are expected to have different average energy and α parameters and to evolve differently in time.

The initial spectra get further processed by flavor transitions, and understanding these oscillations is very important for extracting physics from the detected signal (see Sec. 7.1).

In general, one can describe the neutrino flux as a function of time by specifying the three pinching parameters in successive time slices. Figure 1 gives an example of pinching parameters as a function of time for a specific model, and Fig. 2 shows the spectra for the three flavors as a function of time corresponding to this parameterized description.

3 The Supernova Burst Neutrino Detection Landscape

The burst of neutrinos from the celebrated core-collapse supernova 1987A in the Large Magellanic Cloud, about 50 kpc from Earth, heralded the era of extragalactic neutrino astronomy [12, 13, 14]. The few dozen recorded $\bar{\nu}_e$ events have confirmed the basic physical picture of core collapse and yielded constraints on a wide range of

new physics [15,16]. The community anticipates much more bountiful data and corresponding advances in knowledge when the next nearby star collapses.

Core-collapse supernovae within a few hundred kiloparsecs of Earth— within our own Galaxy and nearby— are quite rare on a human timescale. They are expected once every few decades in the Milky Way (within about 20 kpc), and with a similar rate in Andromeda (about 780 kpc away.) However, core collapses should be common enough to have a reasonable chance of occurring during the few-decades-long lifetime of a typical large-scale neutrino detector. The rarity of these spectacular events makes it all the more critical for the scientific community to be prepared to capture every last bit of information from them.

In principle, the information in a supernova neutrino burst available to neutrino experimentalists is comprised of the flavor, energy and time structure of the several-tens-of-seconds-long, all-flavor, few-tens-of-MeV neutrino burst [17,18]. Imprinted on the neutrino spectrum as a function of time is information about the progenitor, the collapse, the explosion, and the remnant, as well as information about neutrino parameters and potentially exotic new physics. The neutrino energies and flavor content of the burst can be measured only imperfectly due to both the intrinsic nature of the weak interactions of neutrinos with matter and to the imperfect detection resolution of any real detector. For example, supernova burst energies are below CC threshold for ν_μ, ν_τ, $\bar{\nu}_\mu$ and $\bar{\nu}_\tau$ (collectively ν_x), which represent two-thirds of the flux; therefore these flavors are accessible only via NC interactions, which tend to have low cross sections and indistinct detector signatures. These issues make a comprehensive unfolding of neutrino flavor, time and energy structure from the observed interactions a challenging problem.

Much has occurred since 1987, both for experimental and theoretical aspects of supernova neutrino detection. There has been huge progress in the modeling of supernova explosions, and there have been many new theoretical insights about neutrino oscillation and exotic collective effects that may occur in the supernova environment. Experimentally, worldwide detection capabilities have increased enormously, such that there will be orders of magnitude more neutrino interactions from a core collapse at the center of the Galaxy, about 8 kpc away.

3.1 Current Experimental Landscape

At the time of this writing, the 32-kton total mass Super-Kamiokande water Cherenkov detector is the leading supernova neutrino detector; it expects ∼2000-8000 events at 10 kpc [19,20]. Just as for the 1987A sample, these will be primarily $\bar{\nu}_e$ flavor via inverse beta decay (IBD) on free protons. Super-K is being enhanced with the addition of gadolinium as a neutron capture target, which will aid in IBD tagging. IceCube is another water (ice) Cherenkov detector, with a different kind of supernova neutrino sensitivity [21] – it cannot reconstruct individual neutrino events, given that any particular interaction in the ice rarely leads to more than one photoelectron detected. However IceCube can measure the overall supernova neutrino "light curve" as a glow of photons over background counts. Scintillator detectors, made of hydrocarbon, also have high IBD rates. There are several kton-scale scintillator detectors online currently: KamLAND [22], LVD [23], and Borexino [24]. There is one small lead-based detector, HALO [25], with ν_e sensitivity. Some surface or near-surface detectors will also usefully record counts even in the presence of significant cosmogenic background; these include NOvA [26], Daya Bay [27], and Micro-BooNE [28].

In the world's current supernova neutrino flavor sensitivity portfolio [29,17], the sensitivity is primarily to $\bar{\nu}_e$ flavor, via IBD. There is only minor sensitivity to the ν_e component of the flux, which carries with it particularly interesting information (e.g., neutronization burst neutrinos are created primarily as ν_e). While there is some ν_e sensitivity in other detectors via elastic scattering (ES) on electrons and via subdominant interaction channels on nuclei, statistics are relatively small, and it can be difficult to disentangle the flavor content. NC channels are also of particular interest, given that they provide access to all flavors of the supernova flux; the only way to observe the ν_x component is via NC. NC channels are subdominant in large neutrino detectors and are typically difficult to tag, although scintillator has some sensitivity via NC excitation of ^{12}C as well as elastic scattering on protons. Large-scale dark matter detectors have access to the entire supernova flux via NC coherent elastic neutrino-nucleus scattering (CEvNS) on nuclei, with statistics at the level of ∼10 events per ton at 10 kpc (e.g., [30,31]).

3.2 Projected Landscape in the DUNE Era

The next generation of supernova neutrino detectors will be dominated by Hyper-Kamiokande [32], JUNO [33] and DUNE. Hyper-K and JUNO are sensitive primarily to $\bar{\nu}_e$, and Hyper-K in particular will have potentially enormous statistics. The next-generation long-string water detectors, IceCube Gen-2 [34] and KM3NeT [35], will bring improved burst tim-

ing. New tens-of-ton scale noble liquid detectors such as DARWIN [36] will bring new all-flavor sensitivity via NC CEvNS interactions. To this landscape, DUNE will bring unique ν_e sensitivity via ν_e charged-current (ν_eCC) interactions on argon nuclei. It will offer a new opportunity to measure the ν_e content of the burst with high statistics and good event reconstruction.

The past decade has also brought rapid evolution of multi-messenger astronomy. With the advent of the detection of gravitational waves as well as high-energy extragalactic neutrino detection in IceCube, a broad community of physicists and astronomers are now collaborating to extract maximum information from observation in a huge range of electromagnetic wavelengths, neutrinos, charged particles and gravitational waves. This collaboration resulted in the spectacular multi-messenger observation of a kilonova [37]. The next core-collapse supernova will be potentially an even more spectacular multi-messenger observation. Worldwide neutrino detectors are currently participants in SNEWS, the SuperNova Early Warning System [38], which will be upgraded to have enhanced capabilities over the next few years. Information from DUNE will enhance the SNEWS network's reach.

Neutrino pointing information is vital for prompt multi-messenger capabilities. Only some supernova neutrino detectors have the ability to point back to the source of neutrinos. Imaging water Cherenkov detectors like Super-K can do well at this task via directional reconstruction of neutrino-electron ES events. However, other detectors lack pointing ability due to intrinsic quasi-isotropy of the neutrino interactions, combined with lack of detector sensitivity to final-state directionality. Like Super-K, DUNE is capable of pointing to the supernova via the good tracking ability of its time projection chamber (TPC.)

Supernova neutrino detection is more of a collaborative than a competitive game. The more information gathered by detectors worldwide, the more extensive the knowledge to be gained; the whole is more than the sum of the parts. The flavor sensitivity of DUNE is highly complementary to that of the other detectors and will bring critical information for reconstruction of the entire burst's flavor and spectral content as a function of time [39].

3.3 Beyond Core Collapse

While a core-collapse burst is a known source of low-energy (<100 MeV) neutrinos, there are other potential interesting sources of neutrinos in this energy range. Nearby Type Ia [40, 41] or pair instability supernova [42] events may create bursts as well, although they are expected to be fainter in neutrinos than core-collapse supernovae. Mergers of binary neutron stars and of neutron stars and black holes will be low-energy neutrino sources [43, 44], although the rate of these close enough to detect (i.e., within the Galaxy) will be small. There are also interesting steady-state sources of low-energy neutrinos — in particular, there may still be useful oscillation and solar physics information to extract via measurement of the solar neutrino flux. DUNE will have the unique capability of measuring solar neutrino energies event by event with ν_eCC interactions with large statistics, in contrast to other detectors, which primarily make use of recoil spectra [45, 46]. The technical challenge for solar neutrinos is overcoming radiological and cosmogenic backgrounds, although preliminary studies are promising. The diffuse supernova background neutrinos are another target which have a bit higher energy, but which are much more challenging due to very low event rate. There may also be surprises in store, both from burst and steady-state signals, enabled by unique DUNE liquid argon tracking technology.

4 The DUNE Detector

The DUNE detector is part of the DUNE/Long Baseline Neutrino Facility program, which comprises a GeV-scale, high-intensity neutrino beam produced at Fermilab, a precision near detector at the Fermilab site, and underground liquid argon time projection chambers (LArTPCs) 1300 km away. The DUNE LArTPCs will be located at the Sanford Underground Research Facility in South Dakota at a depth of 1.5 km. Physics goals in addition to supernova burst physics of the DUNE/LBNF program include: measurement of neutrino oscillation in the long-baseline beam, study of atmospheric neutrinos, searches for beyond-the-standard-model physics, and searches for baryon number violation.

DUNE will have four modules of 70-kton liquid argon mass in total of which 40 kton will be fiducial mass (10-kton fiducial mass per module). Note that in principle relevant active mass may exceed the nominal fiducial mass for supernova neutrinos in a burst. DUNE is prototyping two types of LArTPCs. Single-phase (SP) LArTPC technology is designed to have horizontal drift of 3.5 m with wrapped-wire readout including two induction and one charge collection anode planes. Dual-phase (DP) LArTPC technology has vertical drift over 12 meters. At the liquid-gas interface at the top of a DP module, drifted ionization charge is amplified and collected.

Liquid argon scintillates at 128 nm, and in both single-phase and dual-phase technologies, wavelength-

shifted photons will be collected by photodetectors (PD), in addition to ionization charge. For the single-phase design, light-trapping devices called X-ARAPUCAs [47, 48] will be mounted between wire layers. These employ dichroic filters and use silicon photomultipliers for photon sensing. For the dual-phase design, cryogenic wavelength-shifter-coated photomultiplier tubes will be deployed on the bottom of the detector.

Both detector designs should have roughly similar capabilities for low-energy physics. Most studies described here were done under the SP design assumption; however the DP design should provide similar results.

The DUNE/LBNF experimental facility, detectors and overall physics program are described in detail in Ref. [4]. More detail about the SP detector design can be found in Ref. [49] and more detail about the DP detector design can be found in Ref. [50].

5 Low-Energy Events in DUNE

5.1 Detection Channels

Liquid argon has a particular sensitivity to the ν_e component of a supernova neutrino burst, via the dominant interaction, CC absorption of ν_e on ^{40}Ar,

$$\nu_e + {}^{40}\text{Ar} \rightarrow e^- + {}^{40}\text{K}^*, \tag{2}$$

for which the observable is the e^- plus deexcitation products from the excited ^{40}K* final state. Additional channels include a $\bar{\nu}_e$ CC interaction and ES on electrons. Cross sections for the most relevant interactions are shown in Fig. 3. It is worth noting that none of the neutrino-^{40}Ar cross sections in this energy range have been experimentally measured, although several theoretical calculations exist [5, 6]. The uncertainties on the theoretical calculations are not generally quantified, and they may be large.

Another process of interest for supernova detection in liquid argon detectors, not yet fully studied, is NC scattering on Ar nuclei by any type of neutrino: $\nu_X + \text{Ar} \rightarrow \nu_X + \text{Ar}^*$, for which the observable is the cascade of deexcitation gammas from the final state Ar nucleus. A dominant 9.8-MeV Ar* decay line has been recently identified as a spin-flip M1 transition [51]. At this energy the probability of e^+e^- pair production is relatively high, offering a potentially interesting NC tag. Other transitions are under investigation. NC interactions are not included in the studies presented here, although they represent a topic of future investigation.

The predicted event rate from a supernova burst may be calculated by folding expected neutrino flux differential energy spectra with cross sections for the
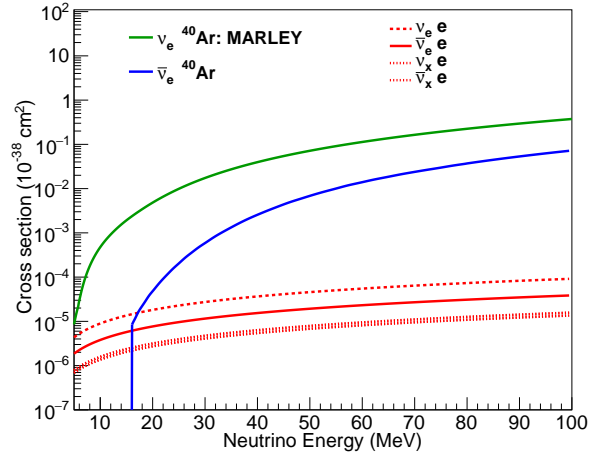

Fig. 3 Cross sections for supernova-relevant interactions in argon [6, 52] as a function of neutrino energy. The ν_e CC cross section shown in green (used for the studies here) is from MARLEY (see Sec. 5.2.1.) Inelastic NC cross sections have large uncertainties and are not shown.

relevant channels, and with detector response; this is done using SNOwGLoBES [6] (see Sec. 5.3.1.)

5.2 Event Simulation and Reconstruction

Supernova neutrino events, due to their low energies, will manifest themselves primarily as spatially small events, perhaps up to a few tens of cm scale, with stub-like tracks from electrons (or positrons from the rarer $\bar{\nu}_e$ interactions). Events from ν_eCC, $\nu_e + {}^{40}\text{Ar} \rightarrow e^- + {}^{40}\text{K}^*$, are likely to be accompanied by de-excitation products — gamma rays and/or ejected nucleons. Gamma rays are in principle observable via energy deposition from Compton scattering, which will show up as small charge blips in the time projection chamber. Gamma rays can also be produced by bremsstrahlung energy loss of electrons or positrons. The critical energy for bremsstrahlung energy loss for electrons in argon is about 45 MeV. Ejected nucleons may result in loss of observed energy for the event, although some may interact to produce observable deexcitations via inelastic scatters on argon. Such MeV-scale activity associated with neutrino interactions has been observed in the ArgoNeuT LArTPC [53]. ES on electrons will result in single scattered electron tracks, and single or cascades of gamma rays may result from NC excitations of the argon nucleus. Each interaction category has, in principle, a distinctive signature. Figure 4 shows examples of simulated ν_eCC and neutrino-electron ES interactions in DUNE.
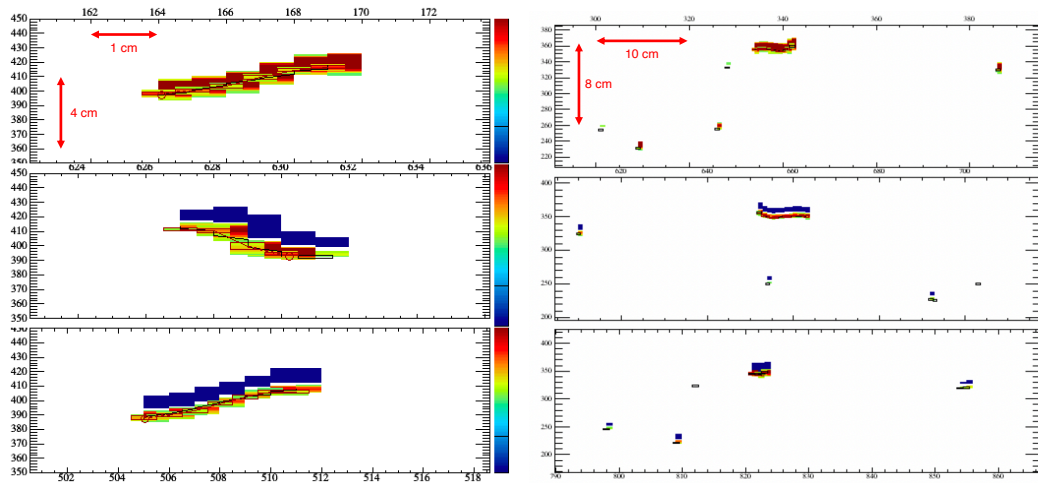
Fig. 4 Left: DUNE event display showing a simulated neutrino-electron ES event (10.25 MeV electron) with track reconstruction. The vertical dimension indicates time and the horizontal dimension indicates wire number. Color represents charge. The top panel shows the collection plane and the bottom panels show induction planes. The boxes represent reconstructed hits. Right: simulated ν_eCC event (20.25 MeV neutrino), showing electron track and blips from Compton-scattered gammas. The events have different spatial scales, as indicated on the figures.

The canonical event reconstruction task is to identify the interaction channel, the neutrino flavor for CC events, and to determine the four-momentum of the incoming neutrino; this overall task is the same for low-energy events as for high-energy ones. The challenge is to reconstruct the properties of the lepton (if present), and to the extent possible, to tag the interaction channel by the pattern of final-state particles. LArSoft [54] open-source event simulation and reconstruction software tools for low-energy events is employed; a full description of the algorithms is beyond the scope of this work. Performance is described in Sec. 5.2.2. Enhanced tools are under development, for example for interaction channel tagging; however, standard tools already provide reasonable capability for energy reconstruction and tracking of low-energy events. Event reconstruction in this energy range has been demonstrated by Micro-BooNE for Michel electrons [55].

5.2.1 Event Generation

MARLEY (Model of Argon Reaction Low Energy Yields) [5] simulates tens-of-MeV neutrino-nucleus interactions in liquid argon. For the studies here, MARLEY was only used to simulate CC ν_e scattering on ^{40}Ar, but other reaction channels will be added in the future.

MARLEY weights the incident neutrino spectrum according to the assumed interaction cross section, selects an initial excited state of the residual ^{40}K* nucleus, and samples an outgoing electron direction using the allowed approximation for the ν_eCC differential cross section, i.e., the zero momentum transfer and zero

nucleon velocity limit of the tree-level ν_eCC differential cross section, which may be written as

$$
\begin{aligned}
\frac{d\sigma}{d\cos\theta} &= \frac{G_F^2 |V_{ud}|^2}{2\pi} |\mathbf{p}_e| \, E_e \, F(Z_f, \beta_e) \\
&\times \left[(1 + \beta_e \cos\theta) B(F) + \left(\frac{3 - \beta_e \cos\theta}{3} \right) B(GT) \right].
\end{aligned}
$$

In this expression, θ is the angle between the incident neutrino and the outgoing electron, G_F is the Fermi constant, V_{ud} is the quark mixing matrix element, $F(Z_f, \beta_e)$ is the Fermi function, and $|\mathbf{p}_e|$, E_e, and β_e are the outgoing electron's three-momentum, total energy, and velocity, respectively. $B(F)$ and $B(GT)$ are the Fermi and Gamow-Teller matrix elements. MARLEY computes this cross section using a table of Fermi and Gamow-Teller nuclear matrix elements. Their values are taken from experimental measurements at low excitation energies and a quasiparticle random phase approximation (QRPA) calculation at high excitation energies.

After simulating the initial two-body ^{40}Ar(ν_e, e^-)^{40}K* reaction for an event, MARLEY also handles the subsequent nuclear de-excitation. For bound nuclear states, the de-excitation gamma rays are sampled using tables of experimental branching ratios [56, 57,58]. These tables are supplemented with theoretical estimates when experimental data are unavailable. For particle-unbound nuclear states, MARLEY simulates the competition between gamma-ray and nuclear fragment[3] emission using the Hauser-Feshbach statistical model. Figure 5 shows an example visualization of

---

[3]Nucleons and light nuclei up to ^{4}He are considered.

a simulated MARLEY event. Figure 6 shows the mean fraction of energy apportioned to the different possible interaction products by MARLEY as a function of neutrino energy.
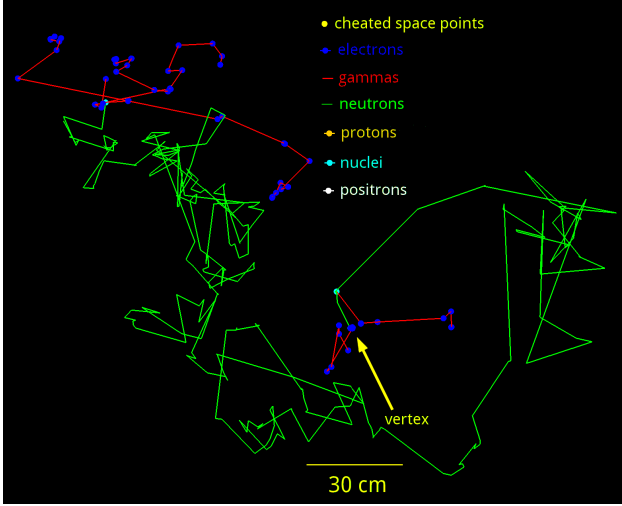

Fig. 5 Visualization of an example MARLEY ν_eCC event simulated in LArSoft, showing the trajectories and energy deposition points of the interaction products.
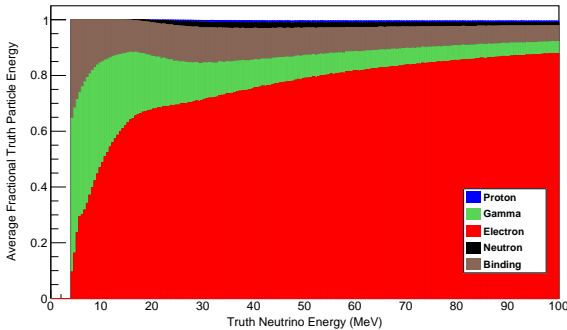

Fig. 6 Fraction of incident neutrino energy going to each final-state particle type in the MARLEY simulation as a function of neutrino energy. "Binding energy" represents the difference in mass of the initial- and final-state nuclei, representing the kinematic threshold for the CC interaction.

5.2.2 Low-energy Event Reconstruction Performance

The LArSoft [54] Geant4-based software package is used to simulate the final-state products from MARLEY in the DUNE LArTPC. Both TPC ionization-based signals and scintillation photon signals are simulated.

For the studies described here, the DUNE LArSoft $1 \times 2 \times 6$ m far detector geometry was used [3], along with standard DUNE reconstruction tools included in the LArSoft package. To determine event-by-event reconstruction information, 2D hits are formed using the HitFinder algorithm. HitFinder scans through wires and defines hits in regions between two signal minima where the maximum signal is above threshold. The algorithm then performs n Gaussian fits for n consecutive regions. The hit center is defined as the fitted Gaussian center, while the beginning and end are defined using the fitted Gaussian width. We used the TrajCluster algorithm to form reconstructed clusters. The TrajCluster algorithm creates clusters using local information from 2D trajectories, taking advantage of minimal ionization energy loss compared to the kinetic energy of the particle. A 2D trajectory is formed from trajectory points defined by the cryostat, plane, and TPC in which the trajectory resides. The trajectory points are made up of charge-weighted positions of all hits used to form the point. The algorithm steps through the 2D space of hits sorted by wire ID number, region of interest in time, and then by "multiplet" (i.e., a collection of hits found using a multi-Gaussian fit). Clusters are formed in the algorithm by stitching together nearby 2D hits. 3D track information is produced using the Projection Matching Algorithm (PMA). PMA takes in 2D clusters formed through TrajCluster, and the algorithm matches clusters in the three 2D projection wire planes to build the tracks. PMA measures the distance between projections, and tracks are formed based on stitching together nearby projections.

The photon (scintillation) simulation implemented ARAPUCA light collection devices with realistic light yields that differ between particle types. Reconstructed photon flashes are used to correct ionization charge loss during drift, which provides substantial improvement to energy reconstruction. Even in the absence of efficient TPC-flash matching, resolution smearing due to drift losses may end up being a small effect, particularly given the high electron lifetimes recently achieved in the DUNE prototype detector [59]. Photons may also be used for calorimetry, although that method has not been implemented for these studies.

Figure 7 shows summarized fractional energy resolution and efficiency performance for MARLEY events. Angular resolution performance will be addressed in a separate publication.

5.2.3 Backgrounds

Understanding of cosmogenic [60] and radiological backgrounds is also necessary for determination of low-energy event reconstruction quality and for setting detector requirements. The dominant radiological is expected to be ^{39}Ar, which β decays at a rate
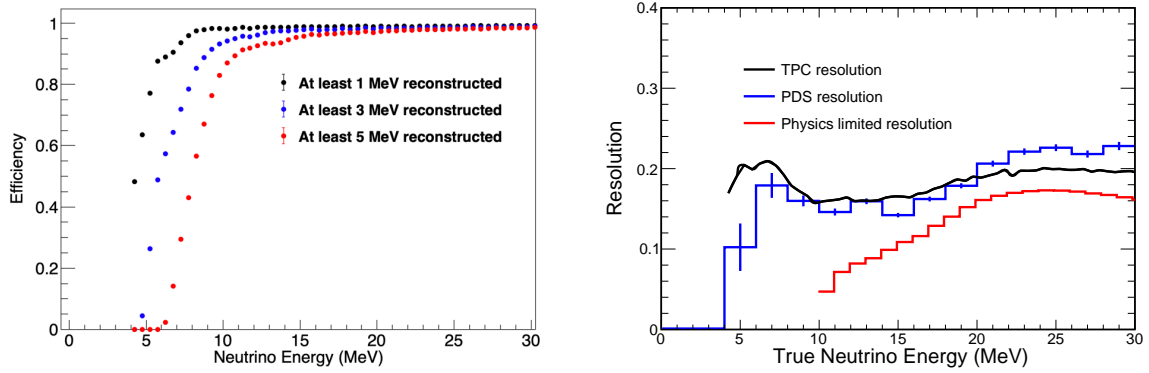
Fig. 7 Left: reconstruction efficiency as a function of neutrino energy for MARLEY ν_eCC events, for different minimum required reconstructed energy. Right: fractional energy resolution (RMS of the distribution of the fractional difference between reconstructed and true energy with respect to true energy) as a function of neutrino energy for TPC tracks corrected for drift attenuation (black) and photon detector calorimetry (blue). The red "physics-limited resolution" is the ratio of the RMS to the mean of the deposited energy distribution, and assumes all energy deposited by final-state particles is reconstructed; the finite resolution represents loss of energy from escaping particles (primarily neutrons). Below 10 MeV the RMS of this distribution is zero.

of $\sim$1 Bq/liter, with an endpoint of <1 MeV. Small single-hit blips from these decays or other radiologicals may fake de-excitation gammas. However preliminary studies show that these background blips will have a very minor effect on reconstruction of triggered supernova burst events. The effects of backgrounds on a data acquisition (DAQ) and triggering system that satisfies supernova burst triggering requirements need separate consideration. These will be the topics of future study. For studies presented here, the impact of backgrounds on event reconstruction is ignored.

5.3 Expected Supernova Burst Signal

5.3.1 SNOwGLoBES

Many supernova neutrino studies done for DUNE so far have employed SNOwGLoBES [6], a fast event-rate computation tool. This uses GLoBES front-end software [61] to convolve fluxes with cross sections and detector parameters. The output is in the form of both mean interaction rates for each channel as a function of neutrino energy and mean "smeared" rates as a function of detected energy for each channel (i.e., the spectrum that actually would be observed in a detector). The smearing (transfer) matrices incorporate both interaction product spectra for a given neutrino energy and detector response. Figure 8 shows examples of such transfer matrices created using MARLEY and LArSoft. They were made by determining the distribution of reconstructed charge using a full simulation of the detector response (including the generation, transport, and detection of ionization signals and the electronics,

followed by high-level reconstruction algorithms) as a function of neutrino energy in 0.5-MeV steps. Each column of a transfer matrix for a given interaction channel represents the detector response to interactions of monoenergetic neutrinos in the detector. An electron drift attenuation correction, which can be computed using the reconstructed photon signal (which determines the time of the interaction and hence the drift distance), improves resolution significantly; see Fig. 9.

Time dependence of a supernova flux in SNOw-GLoBES can be straightforwardly handled by providing multiple fluxes divided into different time bins, although studies here assume a time-integrated flux.

While SNOwGLoBES is, and will continue to be, a fast, useful tool, it has limitations with respect to a full simulation. One loses correlated event-by-event angular and energy information, for example; studies of directionality require such complete event-by-event information [62]. Nevertheless, transfer matrices generated with the best available simulations can be used to compute observed event rates and energy distributions and draw useful conclusions.

5.3.2 Expected Event Rates

Table 1 shows rates calculated for the dominant interactions in argon for the "Livermore" model [63] (included for comparison with literature), the "GKVM" model [64], and the "Garching" electron-capture supernova model [8]. For the first and last, no flavor transitions are assumed in the supernova or Earth; the GKVM model assumes collective effects in the supernova. In general, there is a rather wide variation — up to an order of magnitude — in event rate for different
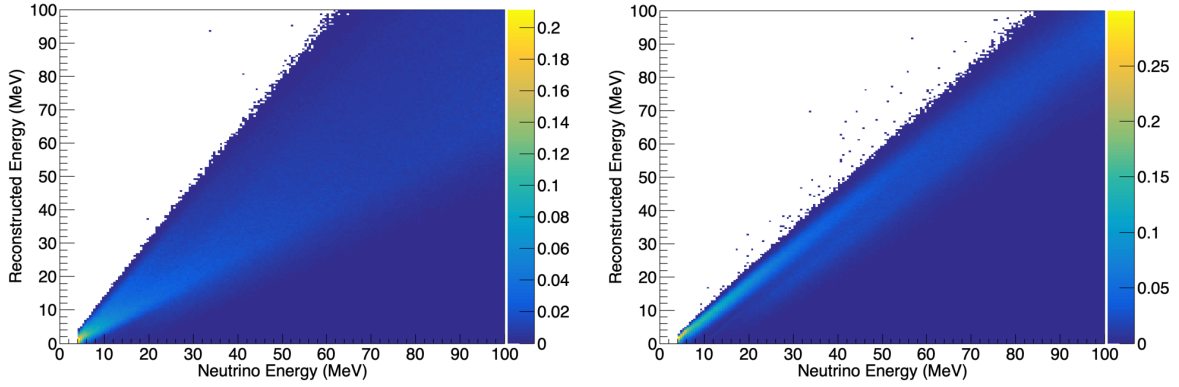
Fig. 8 Left: transfer matrix for SNOwGLoBES created with monoenergetic ν_eCC MARLEY samples run though LArSoft, with the color scale indicating the relative detected charge distribution as a function of neutrino energy. The effects of interaction product distributions and detector smearing are both incorporated in this transfer matrix. The right hand plot incorporates an assumed correction for charge attenuation due to electron drift in the TPC, based on Monte Carlo truth position of the interaction. This correction can be made using PDS information. The drift correction improves energy resolution.
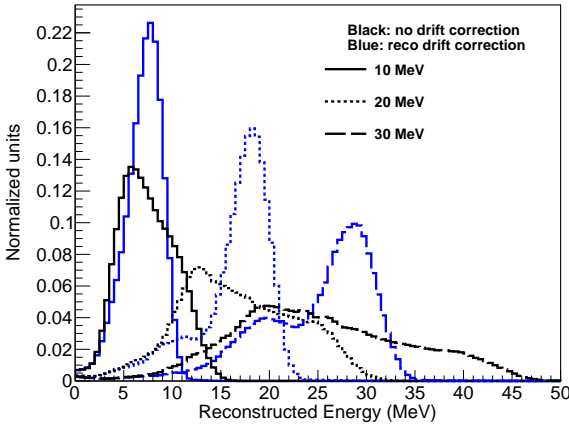
Fig. 9 Observed reconstructed energy distributions for specific interacting neutrino energies (corresponding to columns of the transfer matrices in Fig. 8), with and without reconstructed photon drift correction.

Channel	Livermore	GKVM	Garching
$\nu_e + {}^{40}\text{Ar} \rightarrow e^- + {}^{40}\text{K*}$	2744	3412	918
$\bar{\nu}_e + {}^{40}\text{Ar} \rightarrow e^+ + {}^{40}\text{Cl*}$	224	155	23
$\nu_X + e^- \rightarrow \nu_X + e^-$	341	206	142
Total	3309	3773	1083

Table 1 Event counts computed with SNOwGLoBES for different supernova models in 40 kton of liquid argon for a core collapse at 10 kpc, for ν_eCC and $\bar{\nu}_e$CC channels and ES (X represents all flavors) on electrons. Event rates will simply scale by active detector mass and inverse square of supernova distance. No flavor transitions are assumed for the "Livermore" and "Garching" models; the "GKVM" model includes collective effects. Note that flavor transitions (both standard and collective) will potentially have a large, model-dependent effect, as discussed in Sec. 7.1.

models due to different numerical treatment (e.g., neutrino transport, dimensionality), physics input (nuclear equation of state, nuclear correlation and impact on neutrino opacities, neutrino-nucleus interactions) and flavor transition effects. In addition, there is intrinsic variation in the nature of the progenitor and collapse mechanism. Neutrino emission from the supernova may furthermore have an emitted lepton-flavor asymmetry [65], so that observed rates may be dependent on the supernova direction.

Figure 10 shows the expected event spectrum and the interaction channel breakdown for the "Garching" model before and after detector response smearing with SNOwGLoBES. Clearly, the ν_e flavor dominates. Although water and scintillator detectors will record ν_e events [66,67], the ν_e flavor may not be cleanly separa-

ble in these detectors. Liquid argon is the only future prospect for a large, cleanly tagged supernova ν_e sample [29].

For a given supernova, the number of signal events scales with detector mass and inverse square of distance as shown in Fig. 11. The standard supernova distance is 10 kpc, which is just beyond the center of the Milky Way. At this distance, DUNE will observe from several hundred to several thousand events. For a collapse in the Andromeda galaxy, 780 kpc away, a 40-kton detector would observe a few events at most.

5.4 Burst Triggering

Given the rarity of a supernova neutrino burst in our galactic neighbourhood and the importance of its detection, it is essential to develop a redundant and highly efficient triggering scheme in DUNE. In DUNE, the trig-
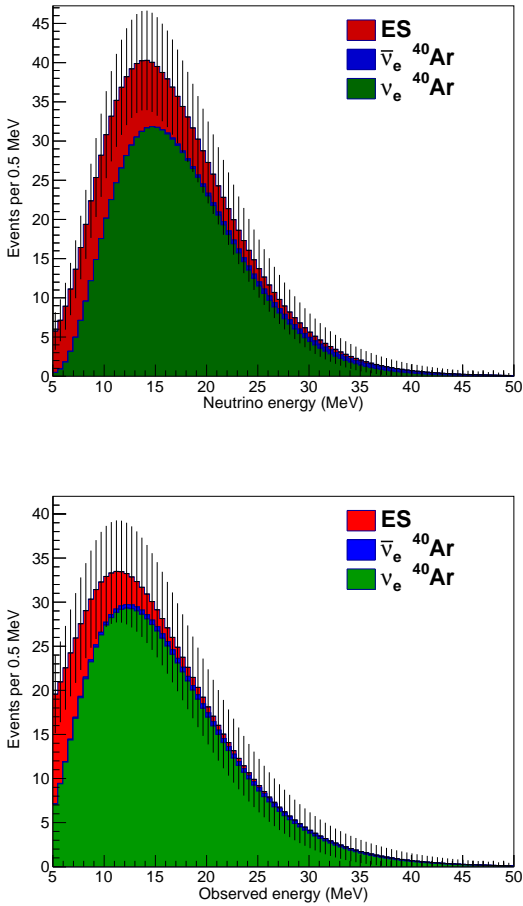
Fig. 10 Top: Spectrum as a function of interacted neutrino energy computed with SNOwGLoBES in 40 kton of liquid argon for the electron-capture supernova [8] ("Garching" model) at 10 kpc, integrated over time, and indicating the contributions from different interaction channels. No oscillations are assumed. Bottom: expected measured spectrum as a function of observed energy, after detector response smearing.

ger on a supernova neutrino burst can be done using either TPC or photon detection system information. In both cases, the trigger scheme exploits the time coincidence of multiple signals over a timescale matching the supernova luminosity evolution. Development of such a data acquisition and triggering scheme is a major activity within DUNE and will be the topic of future dedicated publications. Both TPC and PD information can be used for triggering, for both SP and DP. Here are described two concrete examples of preliminary trigger design studies.

The first example is a trigger based on the photon detection system of the DP module. A real-time algorithm should provide trigger primitives by searching for photomultiplier hits and optical clusters, where the latter combines several hits together based on their time/spatial information. According to simulations, the optimal cluster reconstruction parameters yield a 0.05 Hz radiological background cluster rate for a supernova ν_eCC signal cluster efficiency of 11.8%. Once the optimal cluster parameters are found, the computation of the supernova neutrino burst trigger efficiency is performed using the minimum cluster multiplicity. This value, set by the radiological background cluster rate and the maximum fake trigger rate (one per month), is ≥ 3 in a 2-second window (time in which about half of the events are expected). Approximately $3/0.118 \simeq 25$ interactions must occur in the active volume to obtain approximately 45% trigger efficiency while maintaining a fake trigger rate of one per month.

The triggering efficiency as a function of the number of supernova neutrino interactions is shown in Fig. 12. At 20 kpc, the edge of the Galaxy, about 80 supernova neutrino interactions in the 12.1-kton active mass (assumed supernova-burst-sensitive mass for a single DP module) are expected (see Fig. 11). Therefore, the DP photon detection system should yield a highly efficient trigger for a supernova neutrino burst occurring anywhere in the Milky Way.

The second example considered is a TPC-based supernova neutrino burst trigger in a SP module (SP photon-based triggering will be considered in a future study). Such a trigger considering the time coincidence of multiple neutrino interactions over a period of up to 10 seconds yields roughly comparable efficiencies. Figure 13 shows efficiencies for supernova bursts obtained in this way for a DUNE SP module and for supernova bursts with an energy and time evolution as shown in Fig. 1. Triggering using TPC information is facilitated by a multi-level data selection chain whereby ionization charge deposits are first selected on a per wire basis, using a threshold-based hit finding scheme. This results in low-level trigger primitives (hit summaries) which can be correlated in time and channel space to construct higher-level trigger candidate objects. Low-energy trigger candidates, each consistent with the ionization deposition due to a single supernova neutrino interaction, subsequently serve as input to the supernova burst trigger. Simulations demonstrate that the trigger candidate efficiency for any individual supernova burst neutrino interaction is on the order of 20-30%; see Fig. 13. However, a multiplicity-based supernova burst trigger that integrates low-energy trigger candidates over $\sim$10 s integration window yields high trigger efficiency out to the galactic edge while keeping fake supernova burst trigger rates due to noise and radiological backgrounds to the required level of one per month or less.
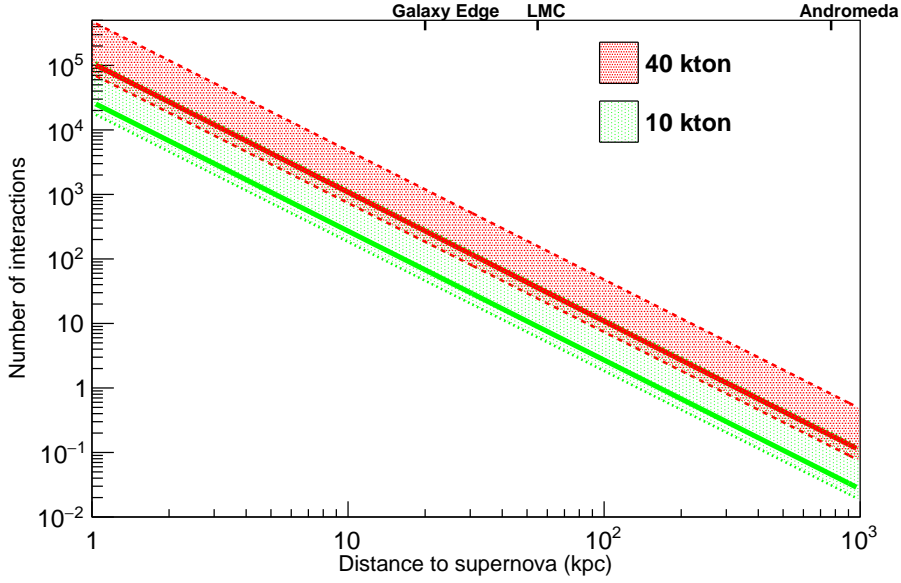
Fig. 11 Estimated numbers of supernova neutrino interactions in DUNE as a function of distance to the supernova, for different detector masses (ν_e events dominate). The red dashed lines represent expected events for a 40-kton detector and the green dotted lines represent expected events for a 10-kton detector. The lines limit a fairly wide range of possibilities for pinched-thermal-parameterized supernova flux spectra (Equation 1) with luminosity 0.5×10^{52} ergs over ten seconds. The optimistic upper line of a pair gives the number of events for average ν_e energy of $\langle E_{\nu_e} \rangle = 12$ MeV, and pinching parameter $\alpha = 2$; the pessimistic lower line of a pair gives the number of events for $\langle E_{\nu_e} \rangle = 8$ MeV and $\alpha = 6$. (Note that the luminosity, average energy and pinching parameters will vary over the time frame of the burst, and these estimates assume a constant spectrum in time. Flavor transitions will also affect the spectra and event rates.) The solid lines represent the integrated number of events for the specific time-dependent neutrino flux model in [8] (see Figs. 1 and 2; this model has relatively cool spectra and low event rates). Core collapses are expected to occur a few times per century, at a most-likely distance of around 10 to 15 kpc.
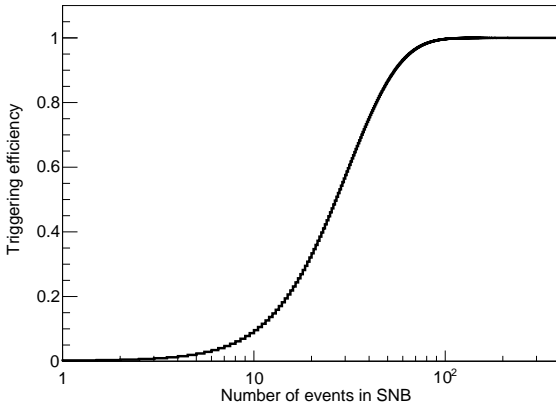
Fig. 12 Supernova neutrino burst triggering efficiency for the DP photon detectors as a function of the number of interactions in one module of the dual phase active volume for the wavelength-shifting reflective half-foil configuration of the baseline design.

An energy-weighted multiplicity count scheme further increases efficiency and minimizes fake triggers due to noise and/or radiological backgrounds. This effect is illustrated in Fig. 13, where a nearly 100% efficiency is possible out to the edge of the galaxy, and 70% efficiency is possible for a burst at the Large Magellanic Cloud (or for any supernova burst creating ~10 events). This performance is obtained by considering the summed-waveform digitized-charge distribution of trigger candidates over 10 s and comparing to a background-only vs. background-plus-burst hypothesis. The efficiency gain compared to a simpler, trigger candidate counting-based approach is significant; using only counting information, the efficiency for a supernova burst at the Large Magellanic Cloud is only 6.5%. These algorithms are being refined to further improve supernova burst trigger efficiency for more distant supernova bursts. Alternative data selection and triggering schemes are also being investigated, involving, e.g., deep neural networks implemented for real-time or online data processing in the DAQ [68].

6 Astrophysics of Core Collapse

A number of astrophysical phenomena associated with supernovae are expected to be observable in the supernova neutrino signal, providing a remarkable window
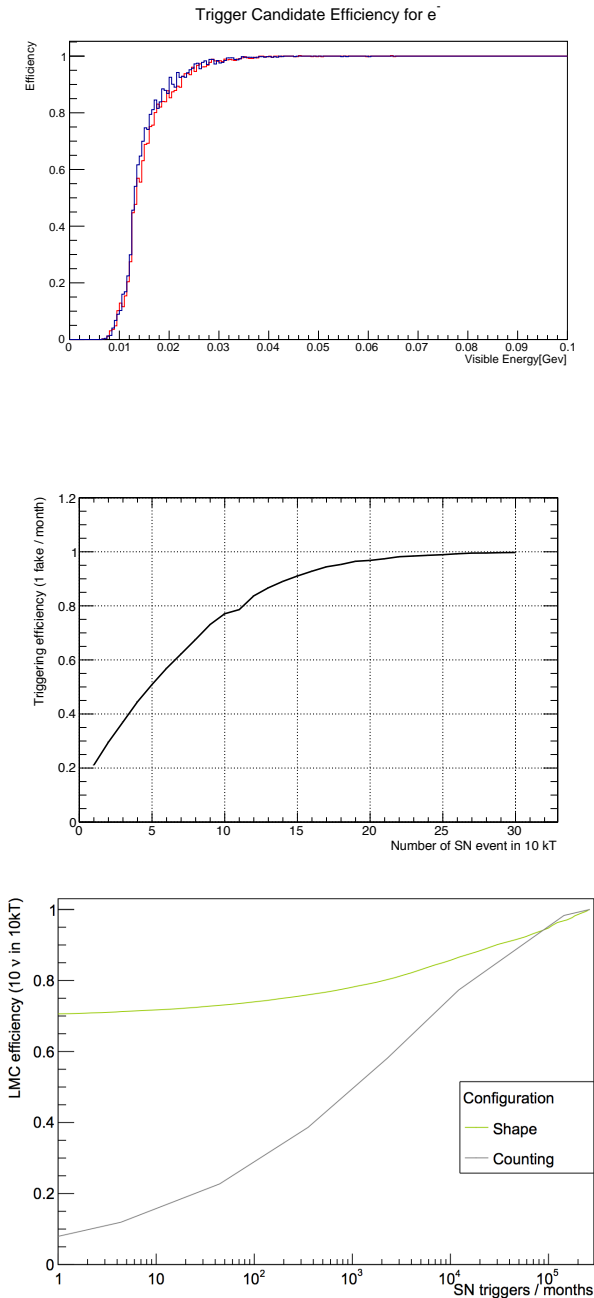
Fig. 13 Top: Single-interaction efficiency for forming trigger candidates from trigger primitives generated online (in blue) and offline (in red), using SP TPC information, as a function of visible energy for electrons such as those from low-energy ν_eCC scattering on argon. Middle: Supernova burst trigger efficiency as a function of the number of supernova neutrino interactions expected in a 10-kton SP module, for a likelihood trigger approach that utilizes sum digitized-charge shape information of trigger candidates input into the trigger decision. Bottom: Supernova burst trigger efficiency as a function of total (signal and fake) trigger bursts per month, for a supernova burst at the Large Magellanic Cloud, where about 10 neutrino interactions are expected in a 10 kton module (see Fig. 11). The efficiency gain with an energy-weighted scheme over a counting-only trigger is significantly improved.

into the event. In particular, the supernova explosion mechanism, which in the current paradigm involves energy deposition into the stellar envelope via neutrino interactions, is still not well understood, and the neutrinos themselves will bring the insight needed to confirm or refute the paradigm.

There are many other examples of astrophysical observables:

- The initial burst, primarily composed of ν_e and called the "neutronization" or "breakout" burst, represents only a small component of the total signal. However, flavor transition effects can manifest themselves in an observable manner in this burst, and flavor transformations can be modified by the "halo" of neutrinos generated in the supernova envelope by scattering [69].
- The formation of a black hole would cause a sharp signal cutoff (e.g., [70,71,72]).
- Shock wave effects (e.g., [73]) would cause a time-dependent change in flavor and spectral composition as the shock wave propagates.
- The standing accretion shock instability (SASI) [74, 75], a "sloshing" mode predicted by three-dimensional neutrino-hydrodynamics simulations of supernova cores, would give an oscillatory flavor-dependent modulation of the flux.
- Turbulence effects [76,77] would also cause flavor-dependent spectral modification as a function of time.

Observation of a supernova neutrino burst in coincidence with gravitational waves (which would also be prompt, and could indeed provide a time reference for a time-of-flight analysis) would be especially interesting [78,79,80,81].

The supernova neutrino burst is prompt with respect to the electromagnetic supernova signal and therefore can be exploited to provide an early warning to astronomers [82,83]. Note that not every core collapse will produce an observable supernova, and observation of a neutrino burst in the absence of an electromagnetic event would be very interesting.

Even non-observation of a burst, or non-observation of a ν_e component of a burst in the presence of supernovae (or other astrophysical events) observed in electromagnetic or gravitational wave channels, would still provide valuable information about the nature of the sources. Furthermore, a long-timescale, sensitive search yielding no bursts will also provide limits on the rate of core-collapse supernovae.

The better one can understand the astrophysical nature of core-collapse supernovae, the easier it will be to extract information about particle physics. DUNE's ca-

pability to characterize the ν_e component of the signal is unique and critical.

6.1 Supernova Flux Parameter Fits

This study investigates how well it will be possible to fit to the supernova pinched-thermal flux parameters, to determine, for example, the ε parameter related to the total binding energy release of the supernova (proportional to the normalization in Eq. 1). Similar studies in the literature for different detectors include e.g., [84, 10,85,86].

The SNOwGLoBES package models neutrino signals described by the pinched-thermal form. A forward-fitting algorithm requiring a SNOwGLoBES-generated energy spectrum for a supernova at a given distance and a chosen "true" set of pinched-thermal parameters $(\alpha^0, \langle E_\nu \rangle^0, \varepsilon^0)$ was developed. As an example, the true parameter values are chosen $(\alpha^0, \langle E_\nu \rangle^0, \varepsilon^0) = (2.5, 9.5, 5 \times 10^{52})$, with $\langle E_\nu \rangle^0$ in MeV and ε in ergs, assumed integrated over a ten-second burst. The study focuses on the ν_e flux and ν_eCC interactions. The algorithm uses this spectrum as a "test spectrum" to compare against a grid of predicted energy spectra generated with many different combinations of $(\alpha, \langle E_\nu \rangle, \varepsilon)$. To quantify these comparisons, the algorithm employs a χ^2 minimization technique to find the best-fit spectrum. The χ^2 function is defined as

$$\chi^2(x) = \sum_{i=1}^{N_b} \frac{\left[N_i(\alpha, \langle E_\nu \rangle, \varepsilon) - N_i(\alpha^0, \langle E_\nu \rangle^0, \varepsilon^0) \right]^2}{\sigma_i^2(x)} \quad (3)$$

In this expression, N_b is the number of bins for the energy spectra, N_i is the number of events in bin i, σ_i is the uncertainty of the contents in bin i (Poisson statistical uncertainty), $(\alpha, \langle E_\nu \rangle, \varepsilon)$ are the set of model parameters used and $(\alpha^0, \langle E_\nu \rangle^0, \varepsilon^0)$ are the model parameters used to generate the test spectrum.

A test spectrum input into the forward-fitting algorithm produces a set of χ^2 values for every element in a grid. While the smallest χ^2 value determines the best fit to the test spectrum, there exist other grid elements that reasonably fit the test spectrum according to their χ^2 values. The collection of these grid elements help determine the expected parameter measurement uncertainty, represented using sensitivity regions in 2D flux parameter space. Three sets of 2D parameter spaces are shown: $(\langle E_\nu \rangle, \alpha)$, $(\langle E_\nu \rangle, \varepsilon)$, and (α, ε).

One point in 2D parameter space encompasses several grid elements, e.g., the $(\langle E_\nu \rangle, \alpha)$ space contains different ε values for a given values of $\langle E_\nu \rangle$ and α. To determine the χ^2 value, ε is profiled over to select the grid element with the smallest χ^2. Sensitivity regions

are determined by placing a cut of $\chi^2 = 4.61$ corresponding to a 90% coverage probability for two free parameters. Figure 14 shows an example of a resulting fit, where for each set of two parameters, the other is profiled over. In this plot, the approximate parameters for three sets of specific models [87,88] are superimposed, to indicate the expected spread for different assumed progenitor masses, equations of state, and simulation codes. A spectral measurement by DUNE would constrain the space of allowed models.

Figures 15 and 16 show the precision with which DUNE can measure two of the spectral parameters, ε, related to the binding energy of the neutron star remnant, and $\langle E_{\nu_e} \rangle$, the average energy of the ν_e component, for the time-integrated spectrum (profiling over α). Figure 15 shows the statistical effect of different assumed supernova distances on determination of the parameters. In Fig. 16, the effect of detector energy resolution is examined. The assumed measured spectrum estimated with SNOwGLoBES takes into account degradation from the neutrino interaction process itself (e.g., energy lost to neutrons), via the MARLEY model. The colored contours in Fig. 16 show increasing levels of assumed detector smearing on the measurement of interaction product energy deposition. For 0% resolution, perfect measurement of the energies of interaction products in the detector is assumed. A 10% measured energy resolution is noticeable but insignificant, and the overall precision on the pinched-thermal flux parameters up to 30% resolution does not change dramatically. According to detector simulation, realistic energy resolution is closest to the 20% level. According to Figs. 15 and 16, in general, the precision of the measurement of supernova spectral parameters (and the ability to constrain supernova models) is limited more strongly by statistics than by energy resolution.

Given the dominance of ν_eCC events in the supernova neutrino sample, particle identification is not a requirement for the primary physics measurements. However, additional capability may be possible by identifying separately NC and ES interactions.

In these studies, we assume that the distance to the core collapse is known. The interpretation of the ε parameter as a binding energy will be affected by uncertainty on the distance.

6.2 Effect of Event Timing

Timing for supernova neutrino events is provided by both the TPC and the photon detector system. Basic timing requirements are set by event vertexing and fiducialization needs. Here we note a few supernova-specific design considerations. During the first 50 ms of
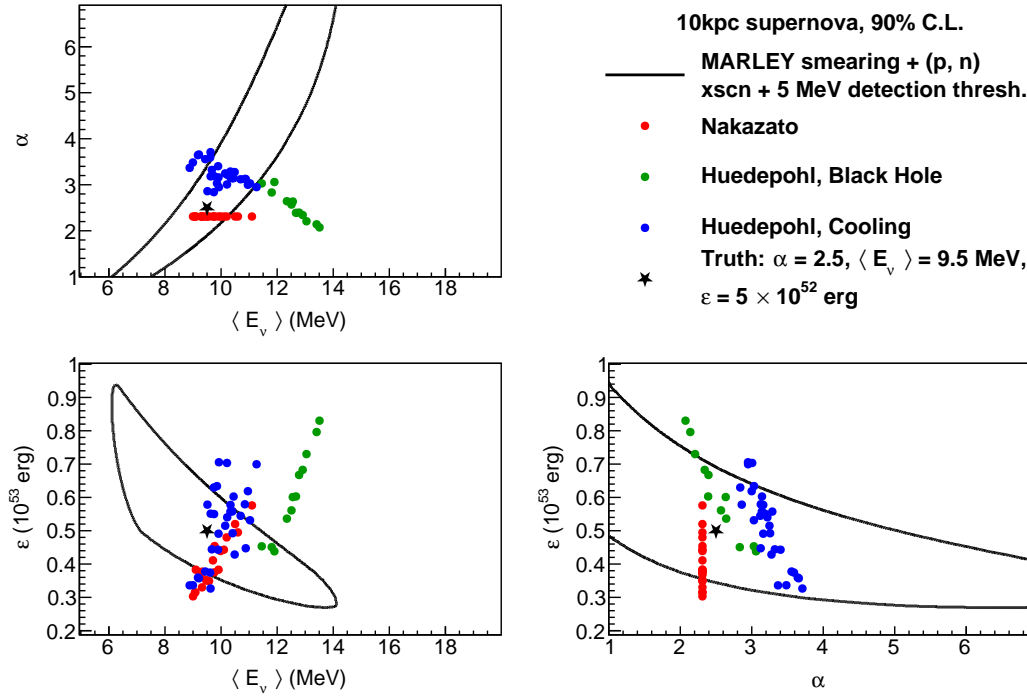
Fig. 14 Sensitivity regions for the three pinched-thermal parameters (90% C.L.). The black star represents the assumed true parameters. SNOwGLoBES assumes a cross section model from MARLEY, realistic detector smearing from LArSoft, and a step efficiency function with a 5-MeV detected energy threshold, for a supernova at 10 kpc. Superimposed are parameters corresponding to the time-integrated flux for three different sets of models: Nakazato [87], Huedepohl black hole formation models, and Huedepohl cooling models [88]. For the Nakazato parameters (for which there is no pinching, corresponding to $\alpha = 2.3$), the parameters are given directly; for the Huedepohl models, they are fit to a time-integrated flux.

a 10-kpc-distant supernova, the mean interval between successive neutrino interactions is $0.5 - 1.7$ ms depending on the model. The TPC alone provides a time resolution of 0.6 ms (corresponding to the drift time at 500 V/cm), commensurate with the fundamental statistical limitations at this distance. However nearly half of galactic supernova candidates lie closer to Earth than this, so the rate can be tens or (less likely) hundreds of times higher. A resolution of <1 μs, as already provided by the photon detector system, ensures that DUNE's measurement of the neutrino burst time profile is always limited by rate and not detector resolution. The hypothesized oscillations of the neutrino flux due to standing accretion shock instabilities would lead to features with a characteristic time of $\sim$10 ms, comfortably greater than the time resolution. The possible neutrino "trapping notch" (dip in luminosity due to trapping of neutrinos in the stellar core) right before the start of the neutronization burst has a width of $1 - 2$ ms. Identifying the trapping notch could be possible for the closest supernovae.

7 Neutrino Physics and Other Particle Physics

A core-collapse supernova is essentially a gravity-powered neutrino bomb: the energy of the collapse is initially stored in the Fermi seas of electrons and neutrinos and then gradually leaked out by neutrino diffusion. The key property of neutrinos that makes them play such a dominant role in the supernova dynamics is the feebleness of their interactions. It then follows that should there be new light (< 100 MeV) particles with even weaker interactions, these could alter the energy transport process and the resulting evolution of the nascent proto-neutron star. Moreover, additional interactions or properties of neutrinos could also be manifested in this way.

Thus, a core-collapse supernova can be thought of as an extremely hermetic system, which can be used to search for numerous types of new physics (e.g., [15,89]). The list includes various Goldstone bosons (e.g., Majorons), neutrino magnetic moments, new gauge bosons ("dark photons"), "unparticles", and extra-dimensional gauge bosons. The existing data from SN1987A already provide significant constraints on these scenarios by confirming the basic energy balance of the explosion.
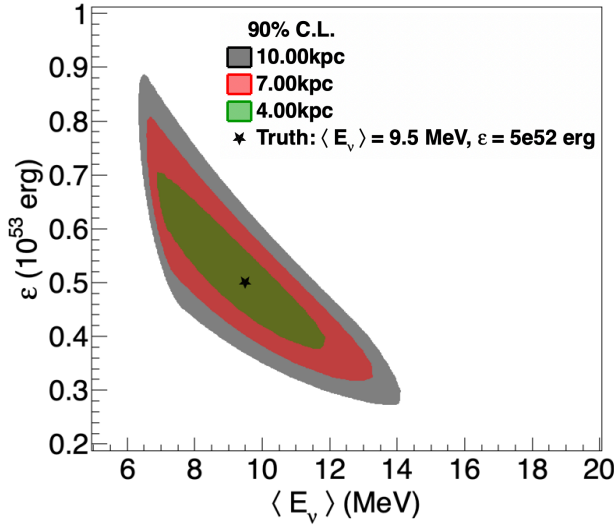
Fig. 15 Sensitivity regions generated in $(\langle E_\nu \rangle, \varepsilon)$ space (profiled over α) for three different supernova distances (90% C.L.). SNOwGLoBES assumes a transfer matrix made using MARLEY with a 20% Gaussian resolution on detected energy, and a step efficiency function with a 5 MeV detected energy threshold.
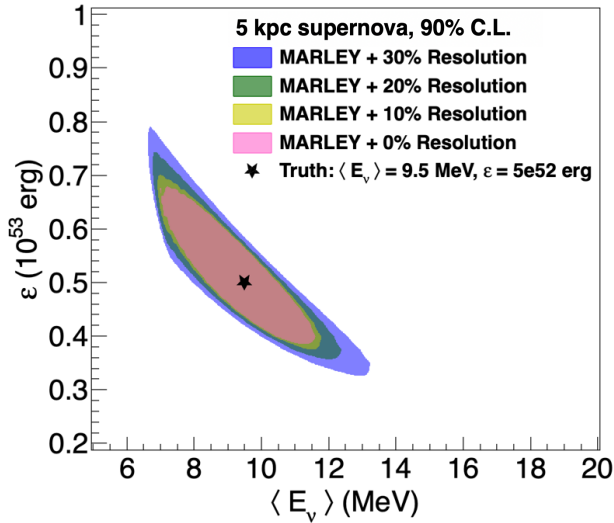

Fig. 16 90% C.L. contours for the luminosity and average ν_e energy spectral parameters for a supernova at 5 kpc. The contours are obtained using the time-integrated spectrum. As discussed in the text, the allowed regions change noticeably but not drastically as one moves from no detector smearing (pink) to various realistic resolutions (wider regions).

At the same time, more precision is highly desirable and will be provided with the next galactic supernova.

Such energy-loss-based analysis will make use of two types of information. First, the total energy of the emitted neutrinos should be compared with the expected release in the gravitational collapse. Note that measurements of all flavors, including ν_e, are needed for the best estimate of the energy release. Second, the rate of

cooling of the protoneutron state should be measured and compared with what is expected from diffusion of the standard neutrinos. The detection of a supernova neutrino burst at DUNE also allows the exploration of corrections to the neutrino velocity that could arise due to violations of Lorentz invariance [90].

Because DUNE is mostly sensitive to ν_e, complementary data from water Cherenkov detector and scintillator for the measurement of $\bar{\nu}_e$ and a careful analysis of the flavor transition pattern will enable inference of the fluxes of μ and τ flavors. As for measuring the energy loss rate, it will require sufficient statistics at late times.

The flavor transition physics and its signatures are a major part of the physics program. Compared to the well-understood case of solar neutrinos, in a supernova, neutrino flavor transformations are much more involved. For supernovae, there are both neutrinos and antineutrinos, and the density profile is such that both mass splittings—"solar" and "atmospheric" — have an effect on the neutrino propagation. While flavor transitions can be reasonably well understood during early periods of the neutrino emission as standard Mikheyev-Smirnov-Wolfenstein (MSW) transitions in the varying density profile of the overlying material, during later periods the physics of the transformations is significantly richer. For example, several seconds after the onset of the explosion, the flavor conversion probability is affected by the expanding shock front and the turbulent region behind it. The conversion process in such a stochastic profile is qualitatively different from the adiabatic MSW effect in the smooth, fixed density profile of the Sun [17].

Even more complexity is brought about by the coherent scattering of neutrinos off each other. This neutrino "self-refraction" results in highly nontrivial flavor transformations close to the neutrinosphere, typically within a few hundred kilometers from the center, where the density of streaming neutrinos is very high. Since the evolving flavor composition of the neutrino flux feeds back into the oscillation Hamiltonian, the problem is nonlinear. Furthermore, as the interactions couple neutrinos and antineutrinos of different flavors and energies, the oscillations are characterized by "collective" modes. This complexity leads to very rich physics that has been the subject of intense interest over the last decade and a voluminous literature exists exploring these collective phenomena, e.g., [91, 92, 93, 94, 95, 96, 97, 98, 99, 100]. This is an active theoretical field and the effects are not yet fully understood. A supernova burst is the only opportunity to study neutrino-neutrino interactions experimentally.

Active-sterile neutrino transitions may also have observable effects [101, 102, 103].

The new effects can imprint information about the inner workings of the explosion on the signal. The flavor transitions can modulate the characteristics of the signal (both event rates and spectra as a function of time). In particular, the flavor transitions can imprint distinctive non-thermal features on the energy spectra, potentially making it possible to disentangle the effects of flavor transformations and the physics of neutrino spectra formation. This in turn should help us learn about the development of the explosion during the crucial first 10 seconds.

7.1 Mass Ordering

The neutrino mass ordering affects the specific flavor composition in multiple ways during the different eras of neutrino emission. References [17, 104] survey in some detail the multiple signatures of mass ordering that will imprint themselves on the flux. For many of these, the ν_e component of the signal will be critical to measure. Some signatures of mass ordering are more robust than others, in the sense that the assumptions are less subject to theoretical uncertainties. One of the more robust of these is the early-time signal, including the neutronization burst. At early times, the matter potential is dominant over the neutrino-neutrino potential, which means that standard MSW effects are in play. The early neutronization-burst period is expected to be dominated by adiabatic MSW transitions driven by the "H-resonance" for $\Delta m_{3\ell}^2$, the larger squared mass difference between mass states, for which the following neutrino-energy-independent relations apply:

$$F_{\nu_e} = F_{\nu_x}^0 \qquad \text{(NO)} , \qquad (4)$$

$$F_{\nu_e} = \sin^2 \theta_{12} F_{\nu_e}^0 + \cos^2 \theta_{12} F_{\nu_x}^0 \qquad \text{(IO)} \qquad (5)$$

and

$$F_{\bar{\nu}_e} = \cos^2 \theta_{12} F_{\bar{\nu}_e}^0 + \sin^2 \theta_{12} F_{\bar{\nu}_x}^0 \qquad \text{(NO)} , \quad (6)$$

$$F_{\bar{\nu}_e} = F_{\bar{\nu}_x}^0 \qquad \text{(IO)} \quad (7)$$

where Fs are the fluxes corresponding to the respective flavors, and the ^{0} superscript represents flux before transition. In this case, for the normal ordering (NO), the neutronization burst, which is emitted as nearly pure ν_e, is strongly suppressed, whereas for the inverted ordering (IO), the neutronization burst is only partly suppressed. Figure 17 shows an example of this effect for a specific model. The same MSW-dominated transitions also affect the subsequent rise of the signal over a fraction of a second; here the time profile will depend on the turn-on of the non-ν_e flavors. For this model there are statistically-significant differences in the time profile of the signal for the different orderings.

Of course, if the mass ordering is already known, one can turn the question around and use the terrestrial determination to better disentangle the other particle physics and astrophysics knowledge from the observed signal.

A detailed investigation of mass-ordering effects over a range of models will be the topic of a future publication.

8 Conclusion

This paper gives an overview of the DUNE experiment's sensitivity to neutrinos with about 5 MeV up to several tens of MeV, the regime of relevance for core-collapse supernova burst neutrinos. This low-energy regime presents particular challenges for triggering and reconstruction. Preliminary DUNE studies show that expected low-energy background rates should not impede efficient detection of nearby supernovae. DUNE's time projection chamber and photon detection systems will both provide information about these events, and DUNE's software tools have enabled preliminary physics and astrophysics sensitivity studies. DUNE will have good sensitivity to the entire Milky Way and possibly beyond, depending on the neutrino luminosity of the core-collapse supernova. According to current understanding, the energy threshold turn-on is a few MeV deposited energy. The energy resolution will be between 10 and 20% in the few tens of MeV range. DUNE will have good sensitivity to supernova ν_e spectral parameters. By exploiting other aspects of a DUNE supernova burst signal, including the time-dependence of its energy and flavor profile and non-thermal spectral features, DUNE has the capability to uncover a broad range of supernova and neutrino physics phenomena, including sensitivity to neutrino mass ordering, collective effects, and potentially many other topics; these will be the subject of future publications.
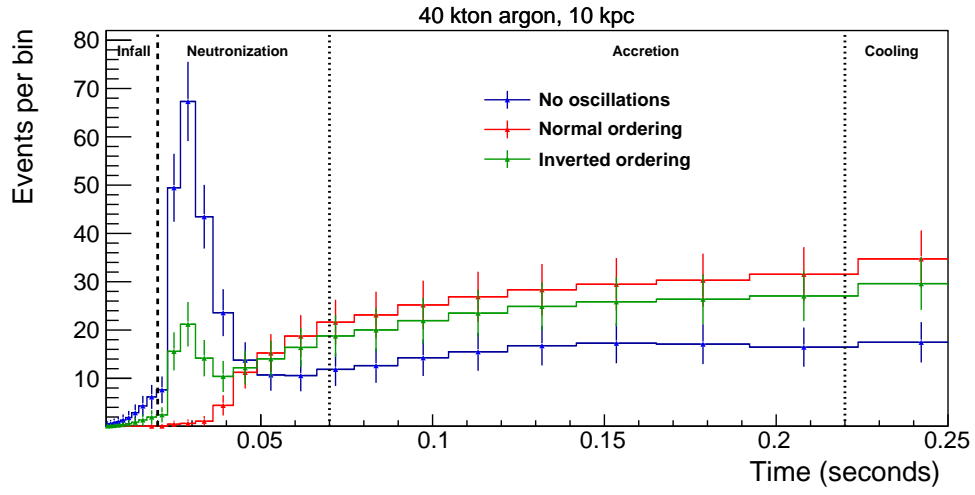
Fig. 17 Expected event rates as a function of time for the electron-capture model in [8] for 40 kton of argon during early stages of the event – the neutronization burst and early accretion phases, for which self-induced effects are unlikely to be important. Shown are: the event rate for the unrealistic case of no flavor transitions (blue) and the event rates including the effect of matter transitions for the normal (red) and inverted (green) orderings. Error bars are statistical, in unequal time bins.

References

1. **DUNE** Collaboration, B. Abi *et al.*, "Deep Underground Neutrino Experiment (DUNE), Far Detector Technical Design Report, Volume I Introduction to DUNE," `arXiv:2002.02967 [physics.ins-det]`.

2. **DUNE** Collaboration, B. Abi *et al.*, "Deep Underground Neutrino Experiment (DUNE), Far Detector Technical Design Report, Volume II DUNE Physics," `arXiv:2002.03005 [hep-ex]`.

3. **DUNE** Collaboration, B. Abi *et al.*, "Deep Underground Neutrino Experiment (DUNE), Far Detector Technical Design Report, Volume IV Far Detector Single-phase Technology," `arXiv:2002.03010 [physics.ins-det]`.

4. **DUNE** Collaboration, B. Abi *et al.*, "The DUNE Far Detector Interim Design Report Volume 1: Physics, Technology and Strategies," `arXiv:1807.10334 [physics.ins-det]`.

5. S. Gardiner, B. Svoboda, C. Grant, and E. Pantic, "MARLEY (Model of Argon Reaction Low Energy Yields).". http://www.marleygen.org/.

6. `http://www.phy.duke.edu/~schol/snowglobes`.

7. E. Braaten and D. Segel, "Neutrino energy loss from the plasma process at all temperatures and densities," *Phys. Rev.* **D48** (1993) 1478–1491, `arXiv:hep-ph/9302213 [hep-ph]`.

8. L. Hudepohl, B. Muller, H.-T. Janka, A. Marek, and G. Raffelt, "Neutrino Signal of Electron-Capture Supernovae from Core Collapse to Cooling," *Phys.Rev.Lett.* **104** (2010) 251101, `arXiv:0912.0260 [astro-ph.SR]`.

9. K. Scholberg, "Neutrinos from supernovae and other astrophysical sources," in *The State of the Art of Neutrino Physics: A Tutorial for Graduate Students and Young Researches*, A. Ereditato, ed., ch. 8, pp. 299–324. World Scientific, 2018.

10. H. Minakata, H. Nunokawa, R. Tomas, and J. W. Valle, "Parameter Degeneracy in Flavor-Dependent Reconstruction of Supernova Neutrino Fluxes," *JCAP* **0812** (2008) 006, `arXiv:0802.1489 [hep-ph]`.

11. I. Tamborra, B. Muller, L. Hudepohl, H.-T. Janka, and G. Raffelt, "High-resolution supernova neutrino spectra represented by a simple fit," *Phys.Rev.* **D86** (2012) 125031, `arXiv:1211.3920 [astro-ph.SR]`.

12. R. Bionta, G. Blewitt, C. Bratton, D. Casper, A. Ciocio, *et al.*, "Observation of a Neutrino Burst in Coincidence with Supernova SN 1987a in the Large Magellanic Cloud," *Phys.Rev.Lett.* **58** (1987) 1494.

13. **KAMIOKANDE-II Collaboration** Collaboration, K. Hirata *et al.*, "Observation of a Neutrino Burst from the Supernova SN 1987a," *Phys.Rev.Lett.* **58** (1987) 1490–1493.

14. E. N. Alekseev, L. N. Alekseeva, V. I. Volchenko, and I. V. Krivosheina, "Possible detection of a neutrino signal on 23 February 1987 at the Baksan Underground Scintillation Telescope of the Institute of Nuclear Research," *JETP Lett.* **45** (1987) 589–592.

15. D. N. Schramm and J. W. Truran, "New physics from Supernova SN1987A," *Phys. Rept.* **189** (1990) 89–126.

16. F. Vissani, "Comparative analysis of SN1987A antineutrino fluence," *J. Phys.* **G42** (2015) 013001, `arXiv:1409.4710 [astro-ph.HE]`.

17. A. Mirizzi, I. Tamborra, H.-T. Janka, N. Saviano, K. Scholberg, R. Bollig, L. Hudepohl, and S. Chakraborty, "Supernova Neutrinos: Production, Oscillations and Detection," *Riv. Nuovo Cim.* **39** no. 1-2, (2016) 1–112, `arXiv:1508.00785 [astro-ph.HE]`.

18. S. Horiuchi and J. P. Kneller, "What can be learned from a future supernova neutrino detection?," *J. Phys.* **G45** no. 4, (2018) 043002, `arXiv:1709.01515 [astro-ph.HE]`.

19. **Super-Kamiokande** Collaboration, M. Ikeda *et al.*, "Search for Supernova Neutrino Bursts at Super-Kamiokande," *Astrophys. J.* **669** (2007) 519–524, `arXiv:0706.2283 [astro-ph]`.

20. **Super-Kamiokande** Collaboration, K. Abe *et al.*, "Real-Time Supernova Neutrino Burst Monitor at Super-Kamiokande," *Astropart. Phys.* **81** (2016) 39–48, `arXiv:1601.04778 [astro-ph.HE]`.

21. **IceCube** Collaboration, R. Abbasi *et al.*, "IceCube Sensitivity for Low-Energy Neutrinos from Nearby Supernovae," *Astron. Astrophys.* **535** (2011) A109, `arXiv:1108.0171 [astro-ph.HE]`. [Erratum: Astron. Astrophys.563,C1(2014)].

22. **KamLAND** Collaboration, K. Eguchi *et al.*, "First results from KamLAND: Evidence for reactor anti-neutrino disappearance," *Phys. Rev. Lett.* **90** (2003) 021802, `arXiv:hep-ex/0212021`.

23. **LVD** Collaboration, N. Y. Agafonova *et al.*, "Implication for the Core-collapse Supernova Rate From 21 Years of Data of the Large Volume Detector," *Astrophys. J.* **802** no. 1, (2015) 47, `arXiv:1411.1709 [astro-ph.HE]`.

24. M. E. Monzani, "Supernova neutrino detection in Borexino," *Nuovo Cim.* **C29** (2006) 269–280.

25. C. A. Duba *et al.*, "HALO: The helium and lead observatory for supernova neutrinos," *J. Phys. Conf. Ser.* **136** (2008) 042077.

26. **NOvA** Collaboration, M. Acero *et al.*, "Supernova neutrino detection in NOvA," `arXiv:2005.07155 [physics.ins-det]`.

27. H. Wei, L. Lebanowski, F. Li, Z. Wang, and S. Chen, "Design, characterization, and sensitivity of the supernova trigger system at Daya Bay," *Astropart. Phys.* **75** (2016) 38–43, `arXiv:1505.02501 [astro-ph.IM]`.

28. **MicroBooNE** Collaboration, J. I. Crespo-Anadón, "The MicroBooNE Continuous Readout Stream for Detection of Supernova Neutrinos," *J. Phys. Conf. Ser.* **1312** no. 1, (2019) 012006, `arXiv:1907.02195 [physics.ins-det]`.

29. K. Scholberg, "Supernova Neutrino Detection," *Ann.Rev.Nucl.Part.Sci.* **62** (2012) 81–103, `arXiv:1205.6003 [astro-ph.IM]`.

30. C. J. Horowitz, K. J. Coakley, and D. N. McKinsey, "Supernova observation via neutrino - nucleus elastic scattering in the CLEAN detector," *Phys. Rev.* **D68** (2003) 023005, `arXiv:astro-ph/0302071 [astro-ph]`.

31. R. F. Lang, C. McCabe, S. Reichard, M. Selvi, and I. Tamborra, "Supernova neutrino physics with xenon dark matter detectors: A timely perspective," *Phys. Rev.* **D94** no. 10, (2016) 103009, `arXiv:1606.09243 [astro-ph.HE]`.

32. **Hyper-Kamiokande** Collaboration, K. Abe *et al.*, "Hyper-Kamiokande Design Report," `arXiv:1805.04163 [physics.ins-det]`.

33. **JUNO** Collaboration, F. An *et al.*, "Neutrino Physics with JUNO," *J. Phys.* **G43** no. 3, (2016) 030401, `arXiv:1507.05613 [physics.ins-det]`.

34. **IceCube** Collaboration, M. G. Aartsen *et al.*, "IceCube-Gen2: A Vision for the Future of Neutrino

Astronomy in Antarctica," `arXiv:1412.5106 [astro-ph.HE]`.

35. **KM3Net** Collaboration, S. Adrian-Martinez *et al.*, "Letter of intent for KM3NeT 2.0," *J. Phys.* **G43** no. 8, (2016) 084001, `arXiv:1601.07459 [astro-ph.IM]`.

36. **DARWIN** Collaboration, J. Aalbers *et al.*, "DARWIN: towards the ultimate dark matter detector," *JCAP* **1611** (2016) 017, `arXiv:1606.07001 [astro-ph.IM]`.

37. **GROND, SALT Group, OzGrav, DFN, INTEGRAL, Virgo, Insight-Hxmt, MAXI Team, Fermi-LAT, J-GEM, RATIR, IceCube, CAASTRO, LWA, ePESSTO, GRAWITA, RIMAS, SKA South Africa/MeerKAT, H.E.S.S., 1M2H Team, IKI-GW Follow-up, Fermi GBM, Pi of Sky, DWF (Deeper Wider Faster Program), Dark Energy Survey, MASTER, AstroSat Cadmium Zinc Telluride Imager Team, Swift, Pierre Auger, ASKAP, VINROUGE, JAGWAR, Chandra Team at McGill University, TTU-NRAO, GROWTH, AGILE Team, MWA, ATCA, AST3, TOROS, Pan-STARRS, NuSTAR, ATLAS Telescopes, BOOTES, CaltechNRAO, LIGO Scientific, High Time Resolution Universe Survey, Nordic Optical Telescope, Las Cumbres Observatory Group, TZAC Consortium, LOFAR, IPN, DLT40, Texas Tech University, HAWC, ANTARES, KU, Dark Energy Camera GW-EM, CALET, Euro VLBI Team, ALMA** Collaboration, B. P. Abbott *et al.*, "Multi-messenger Observations of a Binary Neutron Star Merger," *Astrophys. J.* **848** no. 2, (2017) L12, `arXiv:1710.05833 [astro-ph.HE]`.

38. P. Antonioli *et al.*, "SNEWS: The SuperNova Early Warning System," *New J. Phys.* **6** (2004) 114, `arXiv:astro-ph/0406214`.

39. A. Ankowski *et al.*, "Supernova Physics at DUNE," in *Supernova Physics at DUNE Blacksburg, Virginia, USA, March 11-12, 2016*. 2016. `arXiv:1608.07853 [hep-ex]`.

40. W. P. Wright, J. P. Kneller, S. T. Ohlmann, F. K. Roepke, K. Scholberg, and I. R. Seitenzahl, "Neutrinos from type Ia supernovae: The gravitationally confined detonation scenario," *Phys. Rev.* **D95** no. 4, (2017) 043006, `arXiv:1609.07403 [astro-ph.HE]`.

41. W. P. Wright, G. Nagaraj, J. P. Kneller, K. Scholberg, and I. R. Seitenzahl, "Neutrinos from type Ia supernovae: The deflagration-to-detonation transition scenario," *Phys. Rev.* **D94** no. 2, (2016) 025026, `arXiv:1605.01408 [astro-ph.HE]`.

42. W. P. Wright, M. S. Gilmer, C. Fröhlich, and J. P. Kneller, "Neutrino signal from pair-instability supernovae," *Phys. Rev.* **D96** no. 10, (2017) 103008, `arXiv:1706.08410 [astro-ph.HE]`.

43. O. Caballero, G. McLaughlin, R. Surman, and R. Surman, "Detecting neutrinos from black hole neutron stars mergers," *Phys.Rev.* **D80** (2009) 123004, `arXiv:0910.1385 [astro-ph.HE]`.

44. K. Kyutoku and K. Kashiyama, "Detectability of thermal neutrinos from binary-neutron-star mergers and implication to neutrino physics," *Phys. Rev.* **D97** no. 10, (2018) 103001, `arXiv:1710.05922 [astro-ph.HE]`.

45. F. Capozzi, S. W. Li, G. Zhu, and J. F. Beacom, "DUNE as the Next-Generation Solar Neutrino Experiment," `arXiv:1808.08232 [hep-ph]`.

46. A. Ioannisian, A. Smirnov, and D. Wyler, "Scanning the Earth with solar neutrinos and DUNE," *Phys. Rev.* **D96** no. 3, (2017) 036005, `arXiv:1702.06097 [hep-ph]`.

47. G. Cancelo, F. Cavanna, C. O. Escobar, E. Kemp, A. A. Machado, A. Para, E. Segreto, D. Totani, and D. Warner, "Increasing the efficiency of photon collection in LArTPCs: the ARAPUCA light trap," *JINST* **13** no. 03, (2018) C03040, `arXiv:1802.09726 [physics.ins-det]`.

48. A. A. Machado, E. Segreto, D. Warner, A. Fauth, B. Gelli, R. Maximo, A. Pizolatti, L. Paulucci, and F. Marinho, "The X-ARAPUCA: An improvement of the ARAPUCA device," 2018. `arXiv:1804.01407 [physics.ins-det]`.

49. **DUNE** Collaboration, B. Abi *et al.*, "The DUNE Far Detector Interim Design Report, Volume 2: Single-Phase Module," `arXiv:1807.10327 [physics.ins-det]`.

50. **DUNE** Collaboration, B. Abi *et al.*, "The DUNE Far Detector Interim Design Report, Volume 3: Dual-Phase Module," `arXiv:1807.10340 [physics.ins-det]`.

51. A. Hayes. Private communication.

52. I. Gil Botella and A. Rubbia, "Oscillation effects on supernova neutrino rates and spectra and detection of the shock breakout in a liquid argon TPC," *JCAP* **0310** (2003) 009, `arXiv:hep-ph/0307244`.

53. **ArgoNeuT Collaboration** Collaboration, R. Acciarri, C. Adams, J. Asaadi, B. Baller, T. Bolton, C. Bromberg, F. Cavanna, E. Church, D. Edmunds, A. Ereditato, S. Farooq, A. Ferrari, R. S. Fitzpatrick, B. Fleming, A. Hackenburg, G. Horton-Smith, C. James, K. Lang, M. Lantz, I. Lepetic, B. R. Littlejohn, X. Luo, R. Mehdiyev, B. Page, O. Palamara, B. Rebel, P. R. Sala, G. Scanavini, A. Schukraft, G. Smirnov, M. Soderberg, J. Spitz, A. M. Szelc, M. Weber, W. Wu, T. Yang, and G. P. Zeller, "Demonstration of mev-scale physics in liquid argon time projection chambers using argoneut," *Phys. Rev. D* **99** (Jan, 2019) 012002. `https://link.aps.org/doi/10.1103/PhysRevD.99.012002`.

54. `http://larsoft.org`.

55. **MicroBooNE** Collaboration, R. Acciarri *et al.*, "Michel Electron Reconstruction Using Cosmic-Ray Data from the MicroBooNE LArTPC," *JINST* **12** no. 09, (2017) P09014, `arXiv:1704.02927 [physics.ins-det]`.

56. `https://tendl.web.psi.ch/tendl_2019/talys.html`.

57. M. Bhattacharya *et al.*, "Neutrino absorption efficiency of an Ar-40 detector from the beta decay of Ti-40," *Phys. Rev.* **C58** (1998) 3677–3687.

58. M.-K. Cheoun, E. Ha, and T. Kajino, "High-lying excited states in Gamow Teller strength and their roles in neutrino reactions," *Eur. Phys. J. A* **48** (2012) 137.

59. **DUNE** Collaboration, B. Abi *et al.*, "First results on ProtoDUNE-SP liquid argon time projection chamber performance from a beam test at the CERN Neutrino Platform," `arXiv:2007.06722 [physics.ins-det]`.

60. G. Zhu, S. W. Li, and J. F. Beacom, "Developing the MeV potential of DUNE: Detailed considerations of muon-induced spallation and other backgrounds," *Phys. Rev. C* **99** no. 5, (2019) 055810, `arXiv:1811.07912 [hep-ph]`.

61. P. Huber, M. Lindner, and W. Winter, "Simulation of long-baseline neutrino oscillation experiments with GLoBES (General Long Baseline Experiment Simulator)," *Comput.Phys.Commun.* **167** (2005) 195, `arXiv:hep-ph/0407333 [hep-ph]`.

62. Roeth, A. J., "Supernova Neutrino Pointing with DUNE,". `https://indico.cern.ch/event/868940/`

contributions/3813598/attachments/2081577/3496427/
Point_Res_ICHEP_2020_07_AJRoeth.pdf.

63. T. Totani, K. Sato, H. E. Dalhed, and J. R. Wilson, "Future detection of supernova neutrino burst and explosion mechanism," *Astrophys. J.* **496** (1998) 216–225, arXiv:astro-ph/9710203.

64. J. Gava, J. Kneller, C. Volpe, and G. C. McLaughlin, "A dynamical collective calculation of supernova neutrino signals," *Phys. Rev. Lett.* **103** (2009) 071101, arXiv:0902.0317 [hep-ph].

65. I. Tamborra, F. Hanke, H.-T. Janka, B. Mueller, G. G. Raffelt, *et al.*, "Self-sustained asymmetry of lepton-number emission: A new phenomenon during the supernova shock-accretion phase in three dimensions," *Astrophys.J.* **792** (2014) 96, arXiv:1402.5418 [astro-ph.SR].

66. R. Laha and J. F. Beacom, "Gadolinium in water Cherenkov detectors improves detection of supernova ν_e," *Phys.Rev.* **D89** (2014) 063007, arXiv:1311.6407 [astro-ph.HE].

67. R. Laha, J. F. Beacom, and S. K. Agarwalla, "New Power to Measure Supernova ν_e with Large Liquid Scintillator Detectors." arXiv:1412.8425 [hep-ph], 2014.

68. G. Ge, Y. jae Jwa, and G. Karagiorgi, "ML-based triggering for DUNE," DUNE doc 11311, 2018. https://docs.dunescience.org/cgi-bin/private/ShowDocument?docid=11311&asof=2019-7-15.

69. J. F. Cherry, J. Carlson, A. Friedland, G. M. Fuller, and A. Vlasenko, "Halo Modification of a Supernova Neutronization Neutrino Burst," *Phys.Rev.* **D87** (2013) 085037, arXiv:1302.1159 [astro-ph.HE].

70. J. F. Beacom, R. Boyd, and A. Mezzacappa, "Black hole formation in core collapse supernovae and time-of-flight measurements of the neutrino masses," *Phys.Rev.* **D63** (2001) 073011, arXiv:astro-ph/0010398 [astro-ph].

71. T. Fischer, S. C. Whitehouse, A. Mezzacappa, F. K. Thielemann, and M. Liebendorfer, "The neutrino signal from protoneutron star accretion and black hole formation," *Astron. Astrophys.* **499** (2009) 1, arXiv:0809.5129 [astro-ph].

72. S. W. Li, L. F. Roberts, and J. F. Beacom, "Exciting Prospects for Detecting Late-Time Neutrinos from Core-Collapse Supernovae," arXiv:2008.04340 [astro-ph.HE].

73. R. C. Schirato and G. M. Fuller, "Connection between supernova shocks, flavor transformation, and the neutrino signal," arXiv:astro-ph/0205390 [astro-ph].

74. F. Hanke, A. Marek, B. Muller, and H.-T. Janka, "Is Strong SASI Activity the Key to Successful Neutrino-Driven Supernova Explosions?," *Astrophys.J.* **755** (2012) 138, arXiv:1108.4355 [astro-ph.SR].

75. F. Hanke, B. Mueller, A. Wongwathanarat, A. Marek, and H.-T. Janka, "SASI Activity in Three-Dimensional Neutrino-Hydrodynamics Simulations of Supernova Cores," *Astrophys.J.* **770** (2013) 66, arXiv:1303.6269 [astro-ph.SR].

76. A. Friedland and A. Gruzinov, "Neutrino signatures of supernova turbulence." 2006.

77. T. Lund and J. P. Kneller, "Combining collective, MSW, and turbulence effects in supernova neutrino flavor evolution," *Phys. Rev.* **D88** no. 2, (2013) 023008, arXiv:1304.6372 [astro-ph.HE].

78. N. Arnaud, M. Barsuglia, M.-A. Bizouard, V. Brisson, F. Cavalier, *et al.*, "Detection of a close supernova gravitational wave burst in a network of interferometers, neutrino and optical detectors,"

Astropart.Phys. **21** (2004) 201–221, arXiv:gr-qc/0307101 [gr-qc].

79. C. Ott, E. O'Connor, S. Gossan, E. Abdikamalov, U. Gamma, *et al.*, "Core-Collapse Supernovae, Neutrinos, and Gravitational Waves," *Nucl.Phys.Proc.Suppl.* **235-236** (2013) 381–387, arXiv:1212.4250 [astro-ph.HE].

80. B. Mueller, H.-T. Janka, and A. Marek, "A New Multi-Dimensional General Relativistic Neutrino Hydrodynamics Code of Core-Collapse Supernovae III. Gravitational Wave Signals from Supernova Explosion Models," *Astrophys.J.* **766** (2013) 43, arXiv:1210.6984 [astro-ph.SR].

81. A. Nishizawa and T. Nakamura, "Measuring Speed of Gravitational Waves by Observations of Photons and Neutrinos from Compact Binary Mergers and Supernovae," *Phys.Rev.* **D90** no. 4, (2014) 044048, arXiv:1406.5544 [gr-qc].

82. P. Antonioli *et al.*, "SNEWS: The SuperNova Early Warning System," *New J. Phys.* **6** (2004) 114, astro-ph/0406214.

83. K. Scholberg, "The SuperNova Early Warning System," *Astron. Nachr.* **329** (2008) 337–339, arXiv:0803.0531 [astro-ph].

84. I. Gil Botella and A. Rubbia, "Decoupling supernova and neutrino oscillation physics with LAr TPC detectors," *JCAP* **0408** (2004) 001, arXiv:hep-ph/0404151 [hep-ph].

85. A. Nikrant, R. Laha, and S. Horiuchi, "Robust measurement of supernova ν_e spectra with future neutrino detectors," *Phys. Rev.* **D97** no. 2, (2018) 023019, arXiv:1711.00008 [astro-ph.HE].

86. A. Gallo Rosso, F. Vissani, and M. C. Volpe, "What can we learn on supernova neutrino spectra with water Cherenkov detectors?," *JCAP* **1804** no. 04, (2018) 040, arXiv:1712.05584 [hep-ph].

87. K. Nakazato, K. Sumiyoshi, H. Suzuki, T. Totani, H. Umeda, and S. Yamada, "Supernova Neutrino Light Curves and Spectra for Various Progenitor Stars: From Core Collapse to Proto-neutron Star Cooling," *Astrophys. J. Suppl.* **205** (2013) 2, arXiv:1210.6841 [astro-ph.HE].

88. L. Huedepohl, *Neutrinos from the Formation, Cooling and Black Hole Collapse of Neutron Stars.* PhD thesis, Technische Universitat Munchen., 2014. https://wwwmpa.mpa-garching.mpg.de/ccsnarchive/data/Huedepohl2014_phd_thesis/.

89. G. G. Raffelt, "Particle Physics from Stars," *Ann. Rev. Nucl. Part. Sci.* **49** (1999) 163–216, arXiv:hep-ph/9903472.

90. V. A. Kostelecký and M. Mewes, "Neutrinos with Lorentz-violating operators of arbitrary dimension," *Phys. Rev.* **D85** (2012) 096005, arXiv:1112.6395 [hep-ph].

91. H. Duan, G. M. Fuller, and Y.-Z. Qian, "Collective neutrino flavor transformation in supernovae," *Phys.Rev.* **D74** (2006) 123004, arXiv:astro-ph/0511275 [astro-ph].

92. G. L. Fogli, E. Lisi, A. Marrone, and A. Mirizzi, "Collective neutrino flavor transitions in supernovae and the role of trajectory averaging," *JCAP* **0712** (2007) 010, arXiv:0707.1998 [hep-ph].

93. G. G. Raffelt and A. Y. Smirnov, "Self-induced spectral splits in supernova neutrino fluxes," *Phys.Rev.* **D76** (2007) 081301, arXiv:0705.1830 [hep-ph].

94. G. G. Raffelt and A. Y. Smirnov, "Adiabaticity and spectral splits in collective neutrino transformations,"

Phys.Rev. **D76** (2007) 125008, `arXiv:0709.4641 [hep-ph]`.

95. A. Esteban-Pretel, A. Mirizzi, S. Pastor, R. Tomas, G. Raffelt, *et al.*, "Role of dense matter in collective supernova neutrino transformations," *Phys.Rev.* **D78** (2008) 085012, `arXiv:0807.0659 [astro-ph]`.

96. H. Duan and J. P. Kneller, "Neutrino flavour transformation in supernovae," *J.Phys.G* **G36** (2009) 113201, `arXiv:0904.0974 [astro-ph.HE]`.

97. B. Dasgupta, A. Dighe, G. G. Raffelt, and A. Y. Smirnov, "Multiple Spectral Splits of Supernova Neutrinos," *Phys.Rev.Lett.* **103** (2009) 051105, `arXiv:0904.3542 [hep-ph]`.

98. H. Duan, G. M. Fuller, and Y.-Z. Qian, "Collective Neutrino Oscillations," *Ann.Rev.Nucl.Part.Sci.* **60** (2010) 569–594, `arXiv:1001.2799 [hep-ph]`.

99. H. Duan and A. Friedland, "Self-induced suppression of collective neutrino oscillations in a supernova," *Phys.Rev.Lett.* **106** (2011) 091101, `arXiv:1006.2359 [hep-ph]`.

100. M.-R. Wu, Y.-Z. Qian, G. Martinez-Pinedo, T. Fischer, and L. Huther, "Effects of neutrino oscillations on nucleosynthesis and neutrino signals for an 18 $M_\odot$ supernova model," *Phys.Rev.* **D91** no. 6, (2015) 065016, `arXiv:1412.8587 [astro-ph.HE]`.

101. O. Peres and A. Smirnov, "(3+1) spectrum of neutrino masses: A Chance for LSND?," *Nucl. Phys. B* **599** (2001) 3, `arXiv:hep-ph/0011054`.

102. A. Esmaili, O. Peres, and P. D. Serpico, "Impact of sterile neutrinos on the early time flux from a galactic supernova," *Phys.Rev.* **D90** no. 3, (2014) 033013, `arXiv:1402.1453 [hep-ph]`.

103. J. Tang, T. Wang, and M.-R. Wu, "Constraining sterile neutrinos by core-collapse supernovae with multiple detectors," `arXiv:2005.09168 [hep-ph]`.

104. K. Scholberg, "Supernova Signatures of Neutrino Mass Ordering," *J. Phys.* **G45** no. 1, (2018) 014002, `arXiv:1707.06384 [hep-ex]`.